AD-A071 249 NAVAL RESEARCH LAB WASHINGTON DC F/G 4/2
NUMERICAL SIMULATION OF SUDDEN STRATOSPHERIC WARMINGS.(U)
JUN 79 M R SCHOEBERL, D F STROBEL
UNCLASSIFIED NRL-MR-4013 NL

| OF |
AD A071249

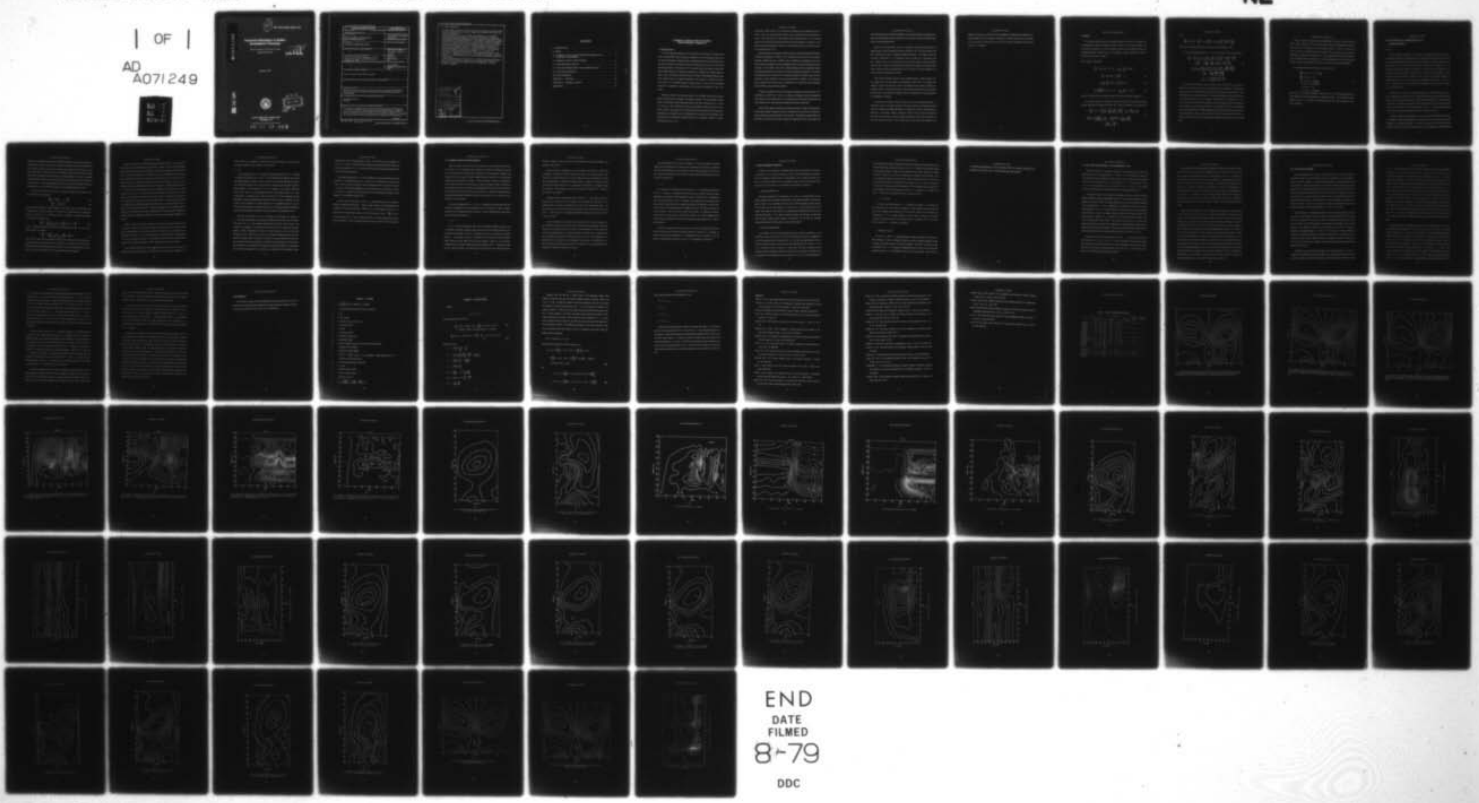

END
DATE FILMED
8-79
DDC

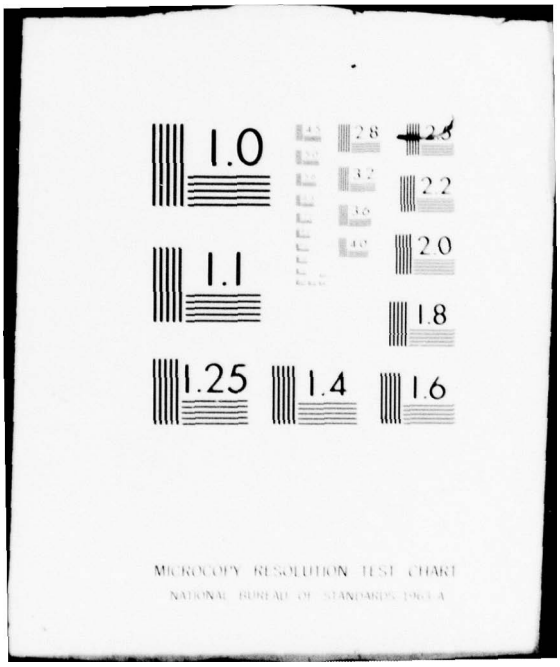
1.0
1.1
1.25
1.4
1.6
2.8
2.2
2.0
1.8
MICROCOPY RESOLUTION TEST CHART
NATIONAL BUREAU OF STANDARDS 1963-A

NRL Memorandum Report 4013

Numerical Simulation of Sudden Stratospheric Warmings

MARK R. SCHOEBERL AND DARRELL F. STROBEL

Plasma Physics Division

June 26, 1979

NAVAL RESEARCH LABORATORY
Washington, D.C.

(14) NRL-MR-4013

SECURITY CLASSIFICATION OF THIS PAGE (When Data Entered)

REPORT DOCUMENTATION PAGE		READ INSTRUCTIONS BEFORE COMPLETING FORM
1. REPORT NUMBER NRL Memorandum Report 4013	2. GOVT ACCESSION NO.	3. RECIPIENT'S CATALOG NUMBER
4. TITLE (and Subtitle) (6) NUMERICAL SIMULATION OF SUDDEN STRATOSPHERIC WARMINGS		5. TYPE OF REPORT & PERIOD COVERED Interim report on a continuing NRL problem 6. PERFORMING ORG. REPORT NUMBER
7. AUTHOR(s) (10) Mark R. Schoeberl and Darrell F. Strobel		8. CONTRACT OR GRANT NUMBER(s)
9. PERFORMING ORGANIZATION NAME AND ADDRESS (9) Memorandum rept.,		10. PROGRAM ELEMENT, PROJECT, TASK AREA & WORK UNIT NUMBERS NRL Problem 67A03-23 and 67A03-30
11. CONTROLLING OFFICE NAME AND ADDRESS Naval Air Systems Command, Washington, D.C. 20361 and National Aeronautics and Space Administration, Washington, D.C. 20546		12. REPORT DATE June 26, 1979 13. NUMBER OF PAGES 74
14. MONITORING AGENCY NAME & ADDRESS(if different from Controlling Office) (16) F52551 (17) WF52551792		15. SECURITY CLASS. (of this report) UNCLASSIFIED 15a. DECLASSIFICATION/DOWNGRADING SCHEDULE N/A
16. DISTRIBUTION STATEMENT (of this Report) Approved for public release; distribution unlimited.		(11) 26 Jun 79 (12) 75p.
17. DISTRIBUTION STATEMENT (of the abstract entered in Block 20, if different from Report)		
18. SUPPLEMENTARY NOTES This research was sponsored partially by Naval Air Systems Command under Subtask WF52-551, Project No. WF52-551-792, and National Aeronautics and Space Administration, Project No. RA40372B(EAF).		
19. KEY WORDS (Continue on reverse side if necessary and identify by block number) Stratospheric warmings Stratosphere		
20. ABSTRACT (Continue on reverse side if necessary and identify by block number) A mechanistic, quasigeostrophic model with a self consistent calculation of the mean zonal flow was used to numerically simulate sudden stratospheric warmings generated by a single zonal harmonic (m) planetary wave. The development of a warming depends critically on the two factors which govern the transmission of planetary waves to the upper stratosphere: (1) the strength of the westerly winds in the lower stratosphere and (2) the magnitude of wave damping in the (Continued)		

DD FORM 1 JAN 73 1473 EDITION OF 1 NOV 65 IS OBSOLETE
S/N 0102-014-6601

SECURITY CLASSIFICATION OF THIS PAGE (When Data Entered)

251 950

20. Abstract (Continued)

same region. Major warmings can only develop when the prewarming lower stratospheric winds are strong. Damping controls the maximum amplitude that a warming can attain and the time constant for its growth rate.

The evolution of $m = 1$ and $m = 2$ warmings are very different. A $m = 1$ warming is characterized by pronounced oscillation of wave amplitude and mean flow that result from resonantly trapped westward propagating planetary waves moving in and out of phase with the tropospherically forced stationary planetary wave. This oscillation can reach sufficient amplitude to decelerate the zonal flow during a cycle to easterlies and create a critical level. Although formation of a mesospheric critical level is not required to initiate a warming, the development and propagation of critical levels in the middle stratosphere atmosphere is central to the evolution of sudden warmings. During a $m = 1$ event the critical level forms initially in the polar region and advances equatorward in its development. But a $m = 2$ critical level first develops in the equatorial region and advances poleward. A $m = 2$ warming is also characterized by a sudden intensification after an initially slow growth in contrast to slowly developing $m = 1$ warmings. Both $m = 1$ and $m = 2$ warmings are accompanied by mesospheric cooling as a result of the induced secondary circulation in response to eddy that transport to the polar stratosphere.

Long term integrations with a steady forced $m = 1$ wave show that the mean flow evolves to a steady, asymptotic state with net cooling in the polar mesosphere from planetary waves. But steady $m = 2$ forcing leads to multiple generation of warmings which are similar to stratospheric vacillations.

CONTENTS

NUMERICAL SIMULATION OF SUDDEN STRATOSPHERIC WARMINGS

I. INTRODUCTION

The most remarkable dynamical event which affects the stratosphere is the sudden stratospheric warming (SSW). Major stratospheric warmings occur on the average every other year in the Northern Hemisphere (Schoeberl, 1978), and during the off years minor warmings are usually observed. Satellite observations indicate that warming events also occur in the Southern Hemisphere (Barnett, 1975; Hartmann, 1977), but these events do not qualify as major warmings by WMO standards. The influence of the SSW is not confined to the middle atmosphere. Quiroz (1977) and McGuirk (1978) showed that the 1976/77 SSW definitely affected tropospheric weather patterns. In addition Ramanathan (1977) argued that the SSW may have a climatic impact on the radiation budget of the polar regions. In view of their meteorological significance a comprehensive understanding of their origin and development is clearly warranted.

Planetary scale eddies, the ultimate energy source for the SSW, are formed in the troposphere through baroclinic, orographic, and diabatic processes. The most important of these eddies at mid-latitudes are large scale quasi-stationary waves with zonal harmonics $m = 1$ and 2 (van Loon et al. 1973). During winter these waves propagate vertically, perturb the stratospheric circulation, and transport heat and momentum from mid-latitudes into the polar regions. Occasionally, a very large planetary wave amplitude pulse is observed in the stratosphere, often associated with the development of blocking patterns in the troposphere. Within 7 to 10 days

Manuscript submitted March 30, 1979.

following the sudden increase in wave amplitude the temperature rises dramatically over the pole as a result of the northward eddy heat flux, and the zonal winds reverse from westerly to easterly. Over single stations at polar latitudes, rocket observations show that the warming appears first at high levels and then descends into the lower stratosphere. During very strong sudden warmings the temperature increase over the polar region may even penetrate deep into the troposphere (Quiroz, 1977).

Previous theoretical investigations of SSW events were reviewed by Schoeberl (1978) and are briefly summarized here. Matsuno (1971) postulated, on the basis of his fairly realistic simulation of SSW events, that a sudden increase in planetary wave amplitude in the troposphere during winter triggers a vertically propagating transient wave which decelerates the mean zonal flow. As the transient wave travels to higher altitudes and lower atmospheric densities the deceleration becomes more pronounced and finally easterlies are generated. The easterly wind region provides a critical level for the stationary planetary waves below which the mean zonal flow is further decelerated. The critical level descends in response to the continuous input of planetary wave energy from the troposphere until it reaches the lower stratosphere where the SSW event becomes fully developed.

In Matsuno's explanation frictional and radiative damping play no importance role in the development of a SSW event. However, the absence of damping prevents the decelerated mean zonal flow from relaxing back to the unperturbed state after eddy forcing ceases and causes planetary waves to be numerically reflected from stationary critical levels.

Geisler (1974), using a one-dimensional mechanistic model of a SSW with realistic damping and lower boundary conditions, noted that the descent of the critical level is often hampered by distortion of the flow ahead of the critical level. This distortion partially reflects the wave before it reaches the critical level, reduces the energy input into the critical region, and

thus slows the descent of the easterly wind region. He also found that the wave amplitude forcing at the lower boundary must be sustained for at least 13 days to initiate a warming in agreement with some observational data.

Holton (1976) studied SSW events with a mechanistic, primitive equation model that included realistic values of damping in contrast to Matsuno's (1971) model and obtained simulated warmings which showed considerably different development. For example, Holton did not obtain a double-layer, $m = 1$ warming and found no evidence for a descending critical level. Instead, after an initial weakening of the mean zonal winds by upward propagancy switch-on pulse, a region of easterlies appeared simultaneously throughout the 30-80 km polar region. Holton also noted a large deceleration of tropical mean zonal winds appeared to be associated with the development of the SSW.

From the above summary and the review by Schoeberl (1978) a number important questions emerge above the mechanisms and development of SSW events. For example, how important is critical level interaction? What is the difference between single and double level warmings? What is the relative importance of forced stationary planetary waves and transient planetary waves? How important is damping? What is the amplitude of the thermal planetary wave imbedded in a warming?

In this paper we attempt to explore and answer some of these important questions. A mechanistic model of the middle atmosphere previously discussed in Schoeberl and Strobel (1978a,b) is adopted and modified specifically to investigate the structure and development of SSW events. This model is similar to Matsuno's (1971) model, but with some important differences namely, realistic frictional and radiative damping and a self consistent calculation of the mean zonal wind structure. We will show that the most critical input parameters that

influence the evolution of a SSW event are the magnitude of damping and the strength of stratospheric winds in the 15-35 km region. Formation of a *mesospheric* critical level is not essential for the occurrence of any SSW. However critical level formation is fundamental to the development of $m = 2$ warmings.

II. MODEL

The zonally averaged circulation of the middle atmosphere (16-130 km) is computed with a quasi-geostrophic, numerical model that explicitly includes a self consistent calculation of solar radiative heating due to O_2 and O_3 absorption, Newtonian cooling, Rayleigh friction, and tropopause boundary conditions based on climatological averages (Schoeberl and Strobel, 1978a; hereafter referred to as Paper I).

This circulation is governed by

$$\frac{\partial \bar{u}}{\partial t} - 2\Omega \sin\theta \bar{v} = \bar{M} - k_r \bar{u} - \frac{1}{a\cos^2\theta} \frac{\partial}{\partial \theta} (\overline{u'v'}\cos^2\theta) \tag{1}$$

$$\frac{\partial \bar{v}}{\partial t} + 2\Omega \sin\theta \bar{u} + \frac{1}{a} \frac{\partial \bar{\phi}}{\partial \theta} = - k_r \bar{v} \tag{2}$$

$$\frac{1}{a\cos\theta} \frac{\partial}{\partial \theta} (\bar{v}\cos\theta) + \frac{1}{p} \frac{\partial}{\partial z} (p\bar{w}) = 0 \tag{3}$$

$$\frac{1}{R} \frac{\partial}{\partial t} \left[\frac{\partial \bar{\phi}}{\partial z} \right] + S\bar{w} = \bar{H} - \alpha \bar{T} - \frac{1}{a\cos\theta} \frac{\partial}{\partial \theta} (\overline{v'T'}\cos\theta) \tag{4}$$

where the variables have their customary meaning. All notation is defined in Appendix A.

The relevant equation for the planetary scale eddies and waves can be derived by scaling Laplaces' tidal equation (Schoeberl and Geller, 1977). Each zonal harmonic (m) is governed by

$$\left[\frac{\partial}{\partial t} + i\bar{\omega}m + k_r \right] \left[\frac{1}{\cos\theta} \frac{\partial}{\partial \theta} \left[\frac{\cos\theta}{\sin^2\theta + \Delta} \frac{\partial \phi'}{\partial \theta} \right] - \frac{m^2 \phi'}{(\sin^2\theta + \Delta)\cos^2\theta} \right] \tag{5}$$

$$\frac{(2\Omega a)^2}{p} \frac{\partial}{\partial z} \left[\frac{p\alpha \partial \phi'}{SR\,\partial z} \right] + \left[\frac{\partial}{\partial t} + i\bar{\omega}m \right] \left[\frac{(2\Omega a)^2}{p} \frac{\partial}{\partial z} \left[\frac{p}{SR} \frac{\partial \phi'}{\partial z} \right] \right]$$

$$+ \frac{im\phi'}{(\sin^2\theta + \Delta)} \frac{\partial \bar{q}}{\partial \theta} = 0$$

where

$$\frac{\partial \bar{q}}{\partial \theta} = 2(\Omega + \bar{\omega}) - \frac{\partial^2 \bar{\omega}}{\partial \theta} + 3 \tan\theta \frac{\partial \bar{\omega}}{\partial \theta} - \sin^2\theta e^z \frac{\partial}{\partial z}\left[\frac{e^{-z}(2\Omega a)^2}{S} \frac{\partial \bar{\omega}}{\partial z}\right]$$

This equation is a slight generalization of the equation used by Matsuno (1971).

For the zonally averaged flow, Eqs. (1)–(5) may be combined to form a single equation

$$\begin{aligned}
&\left[\frac{\partial}{\partial t} + k_r\right] \frac{1}{\cos\theta} \frac{\partial}{\partial \theta} \frac{\cos\theta}{\Delta + \sin^2\theta} \frac{\partial \bar{\phi}}{\partial \theta} + \frac{\partial}{\partial t}\left[\frac{e^z \partial}{\partial z} \frac{e^{-z}(2\Omega a)^2}{SR} \frac{\partial \bar{\phi}}{\partial z}\right] \\
&\quad + \frac{e^z \partial}{\partial z}\left[e^{-z}\alpha \frac{(2\Omega a)^2}{SR} \frac{\partial \bar{\phi}}{\partial z}\right] = \frac{e^z \partial}{\partial z}\left[\frac{e^{-z}(2\Omega a)^2 \bar{H}}{S}\right] \\
&\quad - \frac{1}{2\Omega a^2 \cos\theta} \frac{\partial}{\partial \theta}\left[\frac{1}{\sin\theta}\left\{\frac{1}{\cos\theta} \frac{\partial}{\partial \theta} \frac{\cos\theta}{\sin^2\theta + \Delta}\left[\overline{\frac{\partial \phi'}{\partial \lambda} \frac{\partial \phi'}{\partial \theta}}\right]\right\}\right. \\
&\quad \left. + \frac{e^z \partial}{\partial z} e^{-z} \frac{(2\Omega a)^2}{SR}\left[\overline{\frac{\partial \phi'}{\partial z} \frac{\partial \phi'}{\partial \lambda}}\right]\right] \\
&\quad + \frac{1}{2\Omega a} \frac{1}{\cos\theta} \frac{\partial}{\partial \theta}\left[\frac{\sin\theta\cos\theta}{(\sin^2\theta + \Delta)} \bar{M}\right]
\end{aligned} \tag{6}$$

Given $\bar{H}$, $\bar{M}$, and boundary values for $\bar{\phi}$ and ϕ', Eqs. (5) and (6) form a complete set which may be solved numerically by the method described in Appendix B. The appropriate values of k_r and α for the generation of the mean zonal wind field are given in Paper I. Since the emphasis is on the winter hemisphere at extratropical latitudes, photochemical acceleration of the thermal relaxation rate may be neglected. The quantity $\bar{M}$ is included in Eqs. (1) and (6) to correct the lower stratospheric wind fields which are only weakly forced by ozone absorption of insolation. In the studies by Matsuno (1971) and Holton (1976) a two dimensional mean zonal wind model of the middle atmosphere was constructed from observational data for the initial conditions. Here we calculate $\bar{H}$, infer $\bar{M}$ from observational data, and solve the steady-state form of Eq. (6) without the eddy flux divergence terms to generate the initial wind field.

Figure 1 presents the principal zonal wind fields used in this study. In Fig. 1a the wind field is similar to Matsuno's (1971) initial field and is generated with $\bar{M}$ derived from observational data and k_i increased from the values adopted in Paper I. When the k_i values from Paper I are used, the wind field in Fig. 1b is obtained. If $\bar{M}$ is set equal to zero, then the latter wind field is transformed to the result in Fig. 1c. The essential difference between the Matsuno (1971) and Holton (1976) wind field (Fig. 1a) and the wind field in Fig. 1b is the polar night jet strength. The principal characteristic of Fig. 1c is the weak winds in the lower stratosphere.

The appropriate boundary conditions for Eqs. (5) and (6) are:

$$\begin{aligned}
&\frac{\partial \bar{\phi}}{\partial z} = G(\theta) \text{ at } z = 13.2 \text{ (108km)} \\
&\frac{\partial \bar{\phi}}{\partial \theta} = 0 \text{ at } \theta = \pm \frac{\pi}{2} \\
&\bar{\phi} = E(\theta) \text{ at } z = 0 \text{ (9km)} \\
&\phi' = 0 \text{ at } z = 13.2 \text{ (108km)} \\
&\phi' = 0 \text{ at } \theta = \pm \frac{\pi}{2} \\
&\phi' = F(\theta, t) \text{ at } z = 0 \text{ (9km)}
\end{aligned} \tag{7}$$

where $G(\theta)$ is the radiative equilibrium condition and $E(\theta)$ is the tropopause geopotential height field derived from climatological data as discussed in Paper I. The tropopause forcing of planetary waves, $F(\theta,t)$, is identical to that used by Matsuno (1971) and is applied only to the winter hemisphere.

III. Numerical Results for Undamped Warmings in an Isothermal Atmosphere

a. $m = 1$

Our first numerical experiment was an attempt to reproduce Matsuno's (1971) results. An isothermal atmosphere of 256K was chosen to approximate the static stability of the late winter, high latitude stratosphere. The initial wind field (Fig. 1a) was similar to Matsuno's and damping was set to zero to allow only eddy stress to alter the wind configuration. In the mechanistic model used by Matsuno the generation of a SSW event was accomplished by the switch-on of a geopotential height perturbation over a 5 day period to an asymptotic value of 300 gpm at the lower boundary of 300 mb. With the same lower boundary condition, we obtained the results for a $m = 1$ warming shown as time-height contours for ϕ', $\bar{u}$, $\bar{T}$, and T' in Fig. 2. The associated mean zonal wind profiles with latitude at 10 and 25 days into the simulation are presented in Fig. 3.

From Fig. 2c it is clear that a strong double warming ($\Delta \bar{T} \sim 45$K) is produced after 15-25 days of integration at 30 and 60 km and is accompanied by strong cooling in the upper mesosphere. The zonal wind field develops two easterly regions independently at 100km and 30km associated with the double warming which expand downward and upward to pinch off the polar night jet (cf. Figs. 2b and 3b). The general features of this $m = 1$ double warming resemble closely Matsuno's double warming and would tend to confirm his calculations.

However the upper level warming does *not* occur as a result of critical level descent from the mesosphere as Matsuno hypothesized. An examination of Fig. 2a reveals strong transient oscillations in the middle atmosphere. The switch-on of stationary wave forcing at the lower boundary launches a spectrum of traveling planetary waves that propagate in both longitudinal

directions. The eastward moving waves are probably unimportant since they are evanescent in regions where the mean zonal wind is seen as easterly and decay when the lower boundary forc-

seen as easterly and decay when the lower boundary forcing becomes steady. However, some ing becomes steady. However, some of the westward moving waves can become trapped between the polar night jet and the ground (or the lower boundary in our case). In particular Clark and Schoeberl (1979) found a strong resonantly trapped planetary wave with a period of 15 days for $m = 1$. These traveling planetary waves will move in and out of phase with the stationary planetary wave to produce the oscillation in wave amplitude displayed in Fig. 2a.

To illustrate this point more rigorously let us examine simplified versions of Eqs. (5) and (6), respectively, on the beta plane

$$\left(\frac{\partial}{\partial t} + im\,\bar{\omega}\right) q_m' = -\,v_m'\,\frac{\partial \bar{q}}{\partial y} \tag{8}$$

$$\frac{\partial \bar{q}}{\partial t} = -\,\frac{\partial}{\partial y}\,\overline{(q_m' v_m')} \tag{9}$$

where q represents potential vorticity (Dickinson, 1969; Holton, 1975). The wave motion can be separated into a stationary component (s) with $\exp(im\lambda)$ dependence and a traveling component (τ) with $\exp(im\lambda + i\sigma t)$ dependence where λ is longitude. A straightforward calculation with Eqs. (8) and (9) yields

$$\frac{\partial \bar{q}}{\partial t} = -\,\frac{\partial}{\partial y}\left[\frac{\sigma}{2m\,\bar{\omega}(\sigma + m\,\bar{\omega})}\,\frac{\partial \bar{q}}{\partial y}\,Im\left\{v_s^{*} v_\tau\, e^{i\sigma t}\right\}\right] \tag{10}$$

where $v_{s,\tau}$ denotes the amplitude and phase of the northward wave velocity. If v_s and v_τ are in phase, then Eq. (10) reduces to

$$\frac{\partial \bar{q}}{\partial t} = -\,\frac{\partial}{\partial y}\left[\frac{\sigma}{2m\,\bar{\omega}(\sigma + m\,\bar{\omega})}\,\frac{\partial \bar{q}}{\partial y}\,v_s v_\tau\right]\sin\sigma t \tag{11}$$

Thus the mean zonal wind and temperature fields forced by stationary wave-traveling wave interaction oscillate at the frequency of the traveling wave. Although the mean zonal wind is both accelerated and decelerated during each oscillation, the time averaged acceleration is zero except at a critical level in agreement with wave-zonal flow interaction theorems.

Some of the results of the numerical experiment presented in Fig. 2 can now be clearly interpreted in terms of transient wave-stationary wave interaction. After the upward propagating stationary wave front initially decelerates the zonal wind as predicted by Matsuno (1971) and Uryu (1974), the deceleration is continued in the lower stratosphere by the stationary wave-traveling wave interaction expressed by Eq. (10); however once a critical level is established for any wave component, further mean zonal wind deceleration occurs at the wave absorbing critical level, independently of wave-wave interaction. A detailed comparison of Figs. 2a, 2b, and 2c reveals a close correlation of the wave amplitude with $\bar{u}$ and $\bar{T}$ with a time delay consistent with Eq. (11). For example, note the rapid change from strong easterlies to weak westerlies at 65km during the period days 23-28 that follows the rapid decrease in maximum wave amplitude at the same location for the period days 20-25. It should be pointed out that two transient waves with different frequencies could interact in an analogous manner to the stationary wave-traveling wave interaction. A precise determination of the amplitudes and frequencies of the transient waves cannot be made because the mean zonal flow vacillation continuously shifts the fundamental frequencies of these waves and generates additional components.

While the upper level warming at 60km in Fig. 2c more clearly demonstrates transient wave effects in addition to critical level absorption of the stationary wave, the lower stratospheric warming appears to be controlled by critical level deceleration once easterlies have been established (cf. Fig. 2b). Only a very small amplitude transient disturbance is superimposed on this warming. During the evolution of this warming the easterly wind line descends approximately 15 km consistent with Matsuno's (1971) explanation of critical level interaction.

Hirota (1968) and Schoeberl (1978) suggested that thermal planetary wave may be an important observational component of the SSW structure. In Fig. 2d the amplitude of T' at

60°N is shown to be comparable to variations in $\bar{T}$ at the polar stratopause. In the lower level warming its amplitude is only one-fourth of the $\bar{T}$ variation.

b. $m = 2$

The development of the $m = 2$ warming is strikingly different from the $m = 1$ warming as can be seen from Figs. 4 and 5. For $m = 2$ the warming develops explosively after 20 days with a 60K temperature increase in 4 days at 35 km to a maximum of 70K, almost as large as that obtained by Matsuno (1971). We also obtain a relatively weak secondary warming at 60km; otherwise, the basic features of our $m = 2$ warming are very similar to Matsuno's (1971) results. The $m = 2$ wave amplitude (Fig. 4a) is much weaker than the $m = 1$ wave amplitude (Fig. 2a) during the first 15 days. But from day 15 the wave amplitude increases dramatically in the upper stratosphere and reaches a maximum at day 21, followed by a rapid increase in wave amplitude in the upper mesosphere to a comparable maximum on day 24. The zonal wind deceleration is extremely rapid after day 17, and approximately day 20 easterlies appear nearly simultaneously throughout the upper stratosphere and mesosphere (Fig. 4b).

From Fig. 5 the behavior of the $m = 2$ warming can be understood. In contrast to a $m = 1$ warming which generates an equatorward moving critical level (Fig. 3b), the easterly wind region in the $m = 2$ event advances poleward from the tropics as shown in Fig. 5b. The warming occurs suddenly as the poleward moving critical line in the stratosphere intercepts sufficient vertically propagating wave energy to produce easterlies over most of the middle atmosphere (Fig. 5c). Figs. 5b and 5c also reveal a separate descending critical level from the equatorial mesosphere which is formed by the transient wave pulse launched by the switch-on lower boundary condition and contributes to the upper level warming (Fig. 4c). On the basis of other experiments, the development of the equatorial easterly region appears to be independent of the initial wind configuration in the tropics and is a consequence of the divergence of eddy

momentum flux ($\overline{u'v'}$) in equatorial regions. Since $v' \propto m\phi'$, this flux is twice as large for $m = 2$ as for $m = 1$, when ϕ' is comparable. These results are consistent with Holton's (1976) primitive equation simulation of a $m = 2$ warming which likewise produced poleward advancing critical levels from equatorial regions.

The postwarming period for $m = 2$ does not display the pronounced oscillations which are characteristic of traveling planetary waves. The lack of $m = 2$ traveling waves or free modes is consistent with the recent calculations of Clark and Schoeberl (1979), who found no strong $m = 2$ resonances for westward propagating waves with periods between 5 and 50 days. Unlike $m = 1$ waves, $m = 2$ planetary waves experience greater vertical trapping by stratospheric winds (Matsuno, 1970; Schoeberl and Geller, 1976).

In Fig. 4d some characteristics of the $m = 1$ thermal planetary wave are illustrated. Although its amplitude is substantial ($\sim$ 20K), the large variation of $\bar{T}$ would probably swamp its signature in noisy observational data. Unlike the $m = 2$ thermal planetary wave, the $m = 2$ thermal wave has large amplitude spread over the 30-70 km region. Since $T \propto \frac{\partial \phi'}{\partial z}$, the thermal wave structure for $m = 1$ and 2 warming is illustrative of vertical trapping of wave energy by the polar night jet. Greater trapping generates more vertical variation in ϕ' and hence larger T'.

IV. NUMERICAL RESULTS WITH DAMPING

While the results in the previous section can illuminate certain dynamical processes, they do not apply to the real atmosphere where thermal wave energy may be radiated to space and wave-wave interaction can ultimately lead to dissipation of wave momentum. Similarly in the absence of any wave forcing the zonally averaged circulation would return to the prewarming configuration by these dissipative processes. For lack of a precise theoretical, yet computationally economical description of these processes, we adopt the strategy of Paper I and represent these dissipative processes by Newtonian cooling and Rayleigh friction with the same numerical values for both the waves and mean flow as given in Paper I. It should be remembered that the height-dependent damping coefficients determine the relaxation time of the mean flow after cessation of wave eddy stresses.

In this section integrations for $m = 1$ and $m = 2$ warmings are reported which were performed with damping and the initial wind field in Fig. 1b (cf. Section II). Table 1 contains a summary of all the integration reported in this paper. The post warming phase of these integrations will be discussed in Section VI.

a. $m = 1$

The $m = 1$ results are displayed in Figs. 6 and 7 and should be compared with Figs. 2 and 3 to determine the impact of damping. Figure 6a clearly shows that damping reduces the wave amplitude by approximately a factor of 2 and smooths out the wave oscillation to a regular period of $\sim$ 14 days (Figs. 2a and 6a). The period of this traveling wave which is resonantly trapped between the polar night jet and the lower boundary is sensitive to the zonal wind configuration and the boundary condition (Clark and Schoeberl, 1979). A comparison of Figs. 6b and 2b shows that there is less distortion of the mean flow by wave eddy stresses when

damping is included. Thus the period of the traveling wave should be less variable as our numerical results indicate.

With the presence of damping only very weak easterlies are formed at ~100 km (the "mesospheric" critical level) from the transient wave pulse. These easterlies cannot be sustained by the stationary planetary wave stresses along the critical level against the restoring force of damping which is large near the upper boundary. In addition very little wave amplitude reaches this region after day 35 as a consequence of attenuation as it propagates through the stratosphere. The stratospheric critical level at 35 km does not develop until ~ 50 days and then only for a short duration.

At higher altitudes, small warmings initially develop at ~ 65 km (Fig. 6c) clearly not associated with any critical level but exhibiting a close correlation with oscillations in wave amplitude (Figs. 6a and 6b) and disappears after 30 days as the traveling waves decay. The major warming at 35 km is still in its developmental phase at this time [and does not reach its peak of ~ 22 K until day 55]. With damping included this warming takes twice the time and is a factor of 2 weaker.

A close examination of the numerical results indicates that this warming is not due to critical level effects or stationary wave-transient wave interaction but rather damping. With damping present wave-mean flow interaction can lead to a net deceleration of the mean zonal wind. For the linear damping used in our model deceleration by stationary waves is strongest where the wave amplitude is large and the zonal wind is weak (cf. Eq. (5)). The warming occurs in a region where the restoring force of local damping on the mean flow is not sufficient to overcome the planetary wave stresses produced by the convergence of wave energy and momentum. Eventually the zonal flow is decelerated to easterlies.

The thermal planetary wave reaches a maximum of $\sim$ 20 K in the region of the small, high altitude warming produced by stationary wave-traveling wave interaction and is primarily a traveling thermal disturbance. Strong damping of these traveling oscillations in the low altitude, major warming region prevents the growth of large amplitude thermal planetary waves in this type of warming event.

b. $m = 2$

The introduction of damping has the same effects on a $m = 2$ warming as discussed above for the $m = 1$ warming. The warming takes approximately twice as long to develop as without damping and its amplitude is almost decreased by a factor of 2 (Figs. 8 and 9). Damping also slows the explosive growth of the $m = 2$ warming. The development of the poleward advancing critical level initially formed in the equatorial stratosphere is considerably retarded as damping acts to restore the original westerly wind configuration (Fig. 9). The eddy stresses must *sustain* the easterlies as well as *advance* the critical level poleward. The equatorial mesospheric critcal level never really develops or advances (Figs. 9b-9d), since upward propagating waves are blocked by the stratospheric critical level and damping is strong enough at these heights to restore westerlies.

As might be expected from the first experiment, neither the wave amplitude (Fig. 8a) nor the thermal wave (Fig. 8d) exhibit the periodic oscillations so evident in $m = 1$ warmings. In addition, the thermal wave amplitude (T') is considerably less than the increase of $\bar{T}$ at the peak of the warming. But note that prior to day 35, T' is comparable to the change in $\bar{T}$.

V. OTHER NUMERICAL RESULTS

In addition to the introduction of damping there are other input parameters that can play an important role in the evolution of warming. From our previous discussion the strength of the lower stratospheric westerly winds is a strong candidate. Since an induced secondary circulation is an important component in the stratospheric response to eddy heat transport we also anticipate that the static stability of the stratosphere could potentially be important.

a. Nonisothermal Basic State

Numerical experiments were performed for $m = 1$ and $m = 2$ warmings with the static stability evaluated from the globally averaged CIRA (1972) temperature profile. The results are given in Table 1. The overall effect was minor, but the major stratospheric warming occurred 4-5 days earlier for each zonal harmonic. In the case of $m = 2$, the warming was 8 K more intense. Below 28km the static stability of the nonisothermal atmosphere was less than that of isothermal atmosphere. A more vigorous induced secondary mean circulation was generated from the greater available potential energy in the mean flow. The net effect was a stronger warming as measured by $\Delta \bar{T}$ and a faster evolution of the warming.

b. Lower Stratospheric Winds

To investigate the role of lower stratospheric winds an isothermal atmosphere was used and $\bar{M}$ was set equal to zero in Eqs. (1) and (6). This decreased the initial wind configuration in the lower stratosphere from the strength in Fig. 1b to the weak westerlies illustrated in Fig. 1c. From the summary in Table 1, we note that the polar temperature rise ($\bar{T}$) for both $m = 1$ and $m = 2$ is reduced by a factor of three due to weaker winds. This result is consistent with the theoretical analysis of Dickinson (1969b) who showed that the transmission of planetary waves in the presence of strong damping and weak westerlies is very low. The increased absorption of

wave energy near the lower boundary does not initiate a warming in that region because of the imposed $\bar{\phi}$ boundary conditions at 300 mb. For the $m = 2$ simulation the equatorial easterly regions advances poleward, as before, and establishes an easterly regime throughout the middle stratosphere. However very little wave energy penetrates through the weak westerlies to provide a substantial circulation reversal. Also the critical level cannot descend to a lower altitude for reasons discussed above and absorb more wave energy. For $m = 1$ the severe attenuation of planetary wave energy inhibits the development of the pronounced periodic oscillations in the mesosphere which were characteristic of previous $m = 1$ simulations. For example at 70 km $\phi' \sim 126$ dm at day 15, but only 5 dm for its next peak on day 30.

c. $m = 3$ warming

An attempt was made to generate a $m = 3$ warming even though $m = 3$ warmings have never been observed. After 60 days of integration no major warming was produced and the results did not suggest further integration time was warranted. Planetary waves with high zonal wavenumbers ($m > 2$) are strongly trapped by the polar night jet and become increasingly evanescent throughout the bulk of the stratosphere (Charney and Drazin, 1961). Thus the inability to simulate a $m = 3$ warming is not surprising.

d. Mesospheric cooling

For both $m = 1$ and $m = 2$, strong mesospheric cooling accompanies the strong stratospheric warming as a result of the induced secondary circulation and associated adiabatic cooling in response to eddy heat transport to the polar stratosphere. This effect is clearly seen in Figures 6c and 8c. For $m = 1$ the maximum cooling generated near the pole is 12 K in the 80-100 km region while for $m = 2$, the mesosphere cools 22 K in the same region. These values are

in reasonably good agreement with those of Labitzkes (1972) who observed cooling above the stratopuase on the orders of 20 K at high latitudes during a major warming.

VI. LONG TIME INTEGRATIONS: THE ASYMPTOTIC STATE

The previous studies on stratospheric vacillation cycles by Holton and Mass (1976) and Paper I led us to carry out integrations for $m = 1$ and $m = 2$ to 120 and 180 days, respectively, with asymptotic forcing of 300 gpm at 300 mb. Figures 10 and 11 present the representative values of ϕ' and $\bar{u}$ at 120 days for $m = 1$ and 140 days for $m = 2$. At those times $m = 1$ and $m = 2$ are in post warming periods. The structure of ϕ' for $m = 1$ and $m = 2$ show similar maxima in the mesosphere and secondary maxima in the lower stratosphere (Fig. 10).

A comparison of Fig. 11 with the initial wind configuration in Fig. 1b shows that the polar night jet strength is reduced by approximately 8-9 ms^{-1} at its maximum through the action of planetary wave stresses. However the largest changes occur in the lower stratospheric westerlies which are decelerated by $\sim$ 20 ms^{-1} through eddy heat transport by planetary waves into the polar stratosphere. For $m = 1$ the polar temperature increases by 20K at 30 km, but declines by 8K at 80 km as a result of the adiabatic cooling associated with the induced secondary meridional circulation. Similarly for $m = 2$ planetary waves the polar temperature increases by 15K at 30 km, and decreases by 9K at 80 km. Thus planetary waves tend to cool the polar mesosphere rather than heat it as Green (1972) suggested. The computed effects of these waves are somewhat larger than might be expected, since we have used 300 m forcing, about twice the observed monthly mean wave amplitude at 300 mb for January (van Loon et. al., 1973).

In Paper I steady state solutions for planetary waves interacting with the mean zonal flow were found for the $m = 2$ wave. For the $m = 1$ wave a mesospheric critical level was formed after the first iteration and rendered the iterative procedure divergent in our search for a steady state solution. Our present calculations indicate that a steady state $m = 1$ solution does exist, but can only be obtained by time dependent calculations.

Holton and Mass (1976) and Holton and Dunkerton (1978) have noted that the stratospheric vacillation cycle of planetary wave amplitude and mean circulation can occur even if the wave forcing at the lower boundary is steady. The appearance of a second $m = 2$ warming after day 110 and a third warming at day 168 during the integration is certainly suggestive of a vacillation cycle. From Fig. 12 note that each succeeding $m = 2$ warming is slightly weaker than the previous one. Although this integration was extended to 6 months it would appear that an equilibrium solution is attainable only after more than a year's integration. The adjustment process in muliple $m = 2$ warmings is initimately coupled to the lateral motion of the critical level. But this motion was not allowed by the Holton and Mass (1976) model. Thus it is difficult to compare our model with its much more complex treatment of the mean zonal flow with their results.

Unlike Holton and Dunkerton (1978) who suggest the mechanism for the vacillation cycle is transience from the initial switch-on forcing, we find it more plausible to attribute the vacillations to a cyclic formation of critical levels, followed by restoration of the westerlies through damping, and a susequent increase in planetary wave transmission and eddy heat transport to re-establish another critical level. After each critical level is formed in the equatorial regions it moves poleward until it intercepts all of the upward propagating wave energy. In our model the critical level cannot descend to the lower boundary for reasons discussed in Section V. However, in the real atmosphere the critical level could descend into the troposphere to a level which would cut off the source of planetary wave forcing. Thus our artificial lower boundary at the tropopause is not unrealistic. Once the easterly wind regime is established, the topside of the easterly wind region begins to erode as the mean flow is damped and the easterly region eventually becomes thin enough to permit penetration of planetary waves into the upper stratosphere albeit severely attenuated. Damping continues to slowly restore the winds to the prewarming configuration, at which point the entire process repeats itself.

VII. CONCLUDING REMARKS

The linear damping used in our calculations should be accurate in the initial development of a warming. However, once the planetary waves and the changes in the zonally-averaged circulation reach finite amplitude, this approximate representation of damping probably breaks down and leads to unrealistic estimates of the actual effects of radiative damping and frictional dissipation. In the case of Rayleigh friction there may also be a contribution of unknown magnitude that represents planetary wave stresses on the mean flow and is inappropriate for damping of planetary waves. Thus the numerical simulations that were performed with and without damping should be regarded as extreme bounds on the actual development of SSW events in a realistic atmosphere. In spite of this limitation our model clearly delineates many essential dynamical processes that control and differentiate $m = 1$ and $m = 2$ warmings.

The development of a stratospheric warming in the real atmosphere depends critically on two factors: (1) the strength of the westerly winds in the lower stratosphere and (2) the magnitude of wave damping in the same region. These two factors govern the transmission of planetary wave energy to the less dense regions of the stratosphere and mesosphere where warmings originate. Large transmission requires wind velocities greater than 25 ms^{-1} everywhere at midlatitude or negligible damping ($\sim$ 100 day^{-1}). Thus we expect that major warmings will develop only when the prewarming lower stratospheric winds are large. An observational check of this key theoretical result is difficult because most stratospheric wind data is monthly averaged. Over this time period, the possibility that prewarming, warming, and postwarming data remain distinct is remote.

Damping has two obvious, important effects on the evolution of both $m = 1$ and $m = 2$ warmings. It can suppress the maximum amplitude that a warming attains and slow its development. These effects are consistent with Matsuno's (1971) and Geisler's (1974) earlier studies.

For a $m = 1$ warming damping can be the most important factor that results in the convergence of planetary wave heat and momentum fluxes to decelerate the zonal wind, heat the stratosphere, and precipitate the warming. But the most distinctive feature of a $m = 1$ warming is pronounced oscillations with a period of approximately two weeks. These oscillations are the result of resonantly trapped westward propagating planetary waves (Clark and Schoeberl, 1979) moving in and out of phase with the tropospherically forced stationary planetary wave. As a result of the interaction of the stationary and traveling waves, the mean zonal flow oscillates at the traveling wave frequency. This oscillation can reach sufficient amplitude at times to decelerate the zonal flow during a cycle to easterlies and thus create a critical level. In Matsuno's (1971) model, the upper part of the double warming is generated by these oscillations. However, even if a critical level is not formed, the temperature increase associated with the oscillation has the characteristic magnitude of a warming and may be regarded as the initial phase of a $m = 1$ warming. Damping plays the most important role in the later phase of a $m = 1$ warming and can lead to a stronger temperature increase ($\bar{T}$) than the initial, oscillatory phase.

Although formation of a mesospheric critical level is not a required feature of a warming, the development and propagation of critical levels is central to the evolution of the sudden warmings. Initially in a $m = 1$ event the critical level forms in the polar mesopause region and advances equatorward and downward in its development. In sharp contrast the mesospheric critical level in a $m = 2$ warming initially develops in the equatorial mesopause region and advances poleward. This difference is likely due to the greater refraction of the wave energy flow toward the equator by the mean wind field for $m = 2$ than for $m = 1$ (Matsuno, 1970). Similar remarks about the propagation of critical levels applies to their development in the stratosphere. The $m = 1$ critical level initially form in polar regions and grows equatorward, whereas $m = 2$ critical level originates at equatorial latitudes and progresses poleward. Since the

$m = 1$ planetary wave can propagate with larger amplitude into high latitude regions of the stratosphere than a $m = 2$ wave, the convergence of eddy heat flux for $m = 1$ occurs in the more confined polar region and leads to a greater local heating rate than the midlatitude confined, $m = 2$ wave. In addition, the greater trapping of the $m = 2$ wave relative to the $m = 1$ wave by the jet also reduces the eddy heat flux to high latitudes. Thus the initial critical level formation occurs in the polar regions for $m = 1$. Near the equatorial regions both $m = 1$ and $m = 2$ decelerate the mean zonal flow as a result of momentum flux divergence but $m = 2$'s effect is substantially larger since v′ is twice as large for similar amplitude waves. Thus the $m = 2$ warming is dominated by stronger equatorial deceleration of the flow and a poleward moving critical layer.

The other distinctive feature of a $m = 2$ warming (in addition to its poleward advancing, critical level) is the sudden, explosive character of its development even in the presence of damping. Based on our arguments that damping at finite amplitudes is probably unrealistic in our calculations, a growth rate intermediate between the rates exhibited in Figs. 4c and 8c may be appropriate. From our calculations we would infer that $m = 2$ planetary waves must play an essential role in observed warming events that develop suddenly. Labitzke (1977) noted that a $m = 2$ planetary wave appears to be incapable of generating a major warming by itself, but Schoeberl (1978) points out that the interaction of both $m = 1$ and $m = 2$ is observed in most observed warmings. That is, $m = 2$ *does* play some role in warming development, even though the amplitude of $m = 1$ is strongest just prior to the warming.

Consistent with observations, our numerical simulations also predict realistic values of polar mesospheric cooling coincident with a polar stratospheric warming. This is a direct consequence of the induced secondary circulation in response to eddy heat transport to the polar stratosphere which results in adiabatic cooling in the mesosphere. Labitzke (1972) and Hirota and

Barnett (1977) have deduced mesospheric cooling in polar regions from analysis of warming events. Based on our long time integration studies we find that planetary waves through the induced secondary circulation cause a net cooling of the polar mesosphere.

From an observational point of view our calculations also predict a variety of distinctive features that have yet to be confirmed with observational data. They include the need for strong westerlies in the lower stratosphere, the different latitudinal regions of $m = 1$ and $m = 2$ critical level formation, the pronounced $m = 1$ oscillations with a period $\sim$ 15 days (Madden, 1978; Clark and Schoeberl, 1979), the strong thermal planetary wave imbedded in $m = 1$ warmings (Hirota, 1968; Labitzke, 1977; Schoeberl, 1978), and periodic critical level formation in $m = 2$ warmings.

Finally our results suggest that sudden stratospheric warmings, are a necessary part of the overall adjustment process whereby the atmosphere responds to the strong radiative cooling in polar regions during the long winter night. Normally the synoptic scale eddies through well known baroclinic processes in the troposphere and lower stratosphere transport heat polewards to counter-balance radiative cooling. As winter progresses the polar stratosphere cools dramatically and forms the intense polar night jet to maintain thermal wind balance. As this vortex expands downward and intensifies, the synoptic scale, baroclinic waves eventually become evanescent in the lower stratosphere and no longer transport heat poleward to maintain polar stratospheric temperatures. However, in the presence of a strong polar night jet the large scale planetary waves can penetrate through the lower stratosphere with large transmission in spite of damping and transport heat poleward. Thus the burden of maintaining polar stratospheric temperatures against radiative cooling shifts from the synoptic scale to planetary scale waves. The sudden warming is a product of this shift.

Acknowledgements

This research was supported by NAVAIR Block Fund subtask number WF 52-552-713, and the Upper Atmospheric Research Office of the National Aeronautics and Space Administration through Ames Research Center Contract No. A-47997B (DA).

Appendix A — Notation

z = $\ln\left(\frac{p_o}{p}\right)$, where p = pressure, p_o = 300 mb

u, v = eastward and northward wind velocities, respectively

w = $\frac{dz}{dt}$

a = earth's radius

Ω = angular rotation rate of the earth

R = dry air gas constant

θ = latitude

m = zonal wave number

λ = longitude (measured east)

ϕ = geopotential height

$\overline{H}$ = zonally averaged heating rate (departure from global average)

k_r = Rayleigh friction coefficient

α = Newtonian cooling coefficient

S = $\frac{R<T>}{c_p} + \frac{\partial <T>}{\partial z}$, where $<T>$ is the globally averaged temperature and c_p is specific heat at constant pressure

$\overline{M}$ = external momentum sources and sinks

Δ = $(k_r/2\Omega)^2$

$< >$ = globally averaged variable

$\overline{(\ )}$ = zonally averaged variable − $< >$

$(\ )'$ = perturbation from $\overline{(\ )}$

A = $\frac{3}{4}\frac{1}{S^2}\left(\frac{\partial S}{\partial z}\right)^2 + \frac{1}{2S}\left(\frac{\partial S}{\partial z} - \frac{\partial^2 S}{\partial z^2}\right) + \frac{1}{4}$

Appendix B — Numerical Model

Defining

$$\psi = e^{-z/2} S^{-\frac{1}{2}} \phi$$

we can transform Eqs. (5) and (6) to

$$\frac{\partial}{\partial t}[L_1(\bar{\psi}) + L_{2,0}(\bar{\psi})] + F_1\bar{\psi} + F_2\frac{\partial\bar{\psi}}{\partial z} + k_r L_1(\bar{\psi}) + \alpha L_{2,0}(\bar{\psi})$$
$$= -R_1(\bar{M}) - R_2(\bar{H}) + R_3(Im\{\psi'^*[L_1(\psi') + L_{2,m}(\psi')]\}) \tag{B1}$$

$$\frac{\partial}{\partial t}[L_1(\psi') + L_{2,m}(\psi')] + F_1\psi' + F_2\frac{\partial\psi'}{\partial z} + \bar{X}_m\psi' + \alpha L_{2,m}(\psi') + k_r L_1(\psi')$$
$$= 0 \tag{B2}$$

respectively, where

$$L_1 = \frac{(2\Omega a)^2}{S}\left(\frac{\partial^2}{\partial z^2} + A\right)$$

$$L_{2,m} = \frac{1}{\cos\theta}\frac{\partial}{\partial\theta}\left(\frac{\cos\theta}{\sin^2\theta+\Delta}\frac{\partial}{\partial\theta}\right) - \frac{m^2}{\sin^2\theta\cos^2\theta}$$

$$F_1 = \frac{(2\Omega a)^2}{2S^2}\left(S + \frac{\partial S}{\partial z}\right)\frac{\partial\alpha}{\partial z}$$

$$F_2 = \frac{(2\Omega a)^2}{S}\frac{\partial\alpha}{\partial z}$$

$$R_1 = \frac{2\Omega a}{\cos\theta}e^{-z/2}S^{-\frac{1}{2}}\frac{\partial}{\partial\theta}\frac{\cos\theta}{\sin\theta}$$

$$R_2 = (2\Omega a)^2 e^{z/2}S^{-\frac{1}{2}}\frac{\partial}{\partial z}\frac{e^{-z}\bar{H}R}{S}$$

$$\bar{X}_m = \frac{im}{\sin^2\theta}\frac{\partial\bar{q}}{\partial\theta}$$

Equations (B1) and (B2) are a coupled system of time-dependent elliptic partial differential equations which may be solved by standard numerical techniques. Both ψ' and $L_1(\psi') + L_{2,m}(\psi')$ are required to compute the non-linear forcing term in Eq. (B1). An explicit time scheme for Eq. (B2) would yield only $L_1(\psi') + L_{2,m}(\psi')$ and require an inversion of the operator to obtain ψ'. A better choice is an implicit time scheme which utilizes the same inversion. An ideal candidate is the implicit trapezoidal scheme described by Kurihara (1965). Another advantage of this scheme is that the operator inversion required for $L_1 + L_{2,m}$ can be used to compute steady-state solutions to Eq. (B1) without wave forcing as initial conditions for the time-dependent problems. The coupling terms between the wave motion and mean circulation can be made second order accurate in time by computing the wave field at times $\frac{\Delta t}{2}$ different from the mean flow.

If $\xi_1 = L_1(\psi)$ and $\xi_{2,m} = L_{2,m}(\psi)$

Then Eqs. (B1) and (B2) can be written, respectively, as:

$$\bar{\xi}_1^+ + \bar{\xi}_{2,0}^+ + \frac{\Delta t}{2}\left[\alpha\bar{\xi}_{2,0}^+ + k_r\bar{\xi}_1^+ + F_1\bar{\psi}^+ + F_2\frac{\partial\bar{\psi}}{\partial z}^+\right] = \bar{\xi}_1^- + \bar{\xi}_{2,0}^-$$

$$- \frac{\Delta t}{2}\left[\alpha\bar{\xi}_{2,0}^- + k_r\bar{\xi}_1^- + F_1\bar{\psi}^- + F_2\frac{\partial\bar{\psi}}{\partial z}^-\right] - \Delta t\, R_1(\bar{M})^- - \Delta t R_2(\bar{H})^-$$

$$+ \Delta t\; R_3(Im\{\psi'^0{}^*[\xi_1'^0 + \xi_{2,0}'^0]\}) \qquad \text{(B3)}$$

and

$$\xi_1'^0 + \xi_{2,m}'^0 + \frac{\Delta t}{2}\left[\alpha\xi_{2,m}'^0 + k_r\xi_1'^0 + \bar{X}_m^-\psi'^0 + F_1\psi'^0 + F_2\frac{\partial\psi'^0}{\partial z}\right]$$

$$= \xi_1'^- + \xi_{2,m}'^- - \frac{\Delta t}{2}\left[\alpha\xi_{2,m}'^- + k_r\xi_1'^- + \bar{X}_m^-\psi'^- + F_1\psi'^- + F_2\frac{\partial\psi'^-}{\partial z}\right] \qquad \text{(B4)}$$

where superscripts denote the following points in time:

$$( )^{+} = ( )_{t=t_0+\frac{\Delta t}{2}}$$

$$( )^{0} = ( )_{t=t_0}$$

$$( )^{-} = ( )_{t=t_0-\frac{\Delta t}{2}}$$

$$( )^{=} = ( )_{t=t_0-\Delta t}$$

Evaluation of the spatial operators is done on a staggered mesh spaced at 5° from pole to pole with the closest pole points at 87.5°, for $\bar{\psi}$ and 85°, for ψ'. The vertical grid spacing is 0.37 scale heights. The generalized sweepout method developed by Madala (1978) is used to invert the spatial, elliptic operators. The nonlinear forcing of Eq. (B3) restricts the time step to the equivalent leapfrog time scheme limit. To obtain the correct group velocity for planetary waves with the implicit trapezoidal scheme the C.F.L. condition must be satisfied. On the basis of several numerical experiments, the maximum allowable time step was found to be about 0.12 days.

References

Barnett, J.J., 1975: Large sudden warming in the southern hemisphere, *Nature*, **255**, 387-389.

Charney, J.G., and P.G. Drazin, 1961: Propagation of planetary scale disturbances from the lower atmosphere into the upper atmosphere, *J. Geophys. Res.*, **66**, 83-109.

CIRA 1972: COSPAR *International Reference Atmosphere*, Berlin, Akedemie-Verlag, 450 pp.

Clark, J.H.E. and M.R. Schoeberl, 1979: Resonant planetary waves in a spherical atmosphere, submitted to *J. Atmos. Sci.*

Dickinson, R.E., 1969a: Theory of planetary wave zonal flow interaction, *J. Atmos. Sci.*, **26**, 73-81.

Dickinson, R.E., 1969b: Vertical propagation of planetary Rossby waves through an atmosphere with Newtonian cooling, *J. Geophys. Res.*, **74**, 929-938.

Dickinson, R.E., 1973a: Method of parameterization for infrared cooling between altitudes of 30 and 70 kilometers, *J. Geophys. Res.*, **78**, 4451-4457.

Geisler, J. E., 1974: A numerical model of the sudden stratospheric warming mechanism, *J. Geophys. Res.*, **79**, 4989-4999.

Green, J.S.A., 1972: Large scale motion in the upper stratosphere and mesosphere: an evaluation of data and theories. *Phil. Trans. Roy. Soc. Lond.*, **271**, 577-583.

Hartmann, D.L., 1977: Stationary planetary waves in the southern hemisphere, *J. Geophys. Res.*, **82**, 4930-4934.

Hirota, I, 1968: Planetary waves in the upper stratosphere in early 1966, *J. Meteorol. Soc. Japan.*, **46**, 418-430.

Hirota, I. and J.J. Barnett, 1977: Planetary waves in the winter mesosphere — preliminary analysis of Nimbus 6 PMR results, *Quart. J. Roy. Meteorol. Soc.*, **103**, 487-498.

Holton, J.R., 1975: *Dynamic meteorology of the stratosphere and mesosphere, Meteorol. Monogr.*, No. **15**, 216 pp, American Meteorological Society, Boston, Mass.

Holton, J.R., 1976: A semi-spectral numerical model for wave-mean flow interactions in the stratosphere: applications to sudden stratospheric warnings. *J. Atmos. Sci.*, **33**, 1639-1649.

Holton, J.R. and T. Dunkerton, 1978: On the role of wave transcience and dissipation in stratospheric mean flow vacillations, *J. Atmos. Sci.* **85**, 740-744.

Holton, J.R. and C. Mass, 1976: Stratospheric vacillation cycles. *J. Atmos. Sci.*, **33**, 2218-2225.

Kurihara, Y., 1965: On the use of implicit and iterative methods for time integration of the wave equation, *Mon. Wea. Rev.*, **93**, 33-46.

Labitzke, K, 1972: The interaction between the stratosphere and mesosphere in winter, *J. Atmos. Sci.*, **29**, 1395-1399.

Labitzke, K., 1977: Interannual variability of the winter stratosphere in the Northern Hemisphere, *Mon. Weather Rev.*, **105**, 762-770.

Madala, R., 1978: An efficient direct solver for separable and non-separable elliptic equations, *Mon. Wea. Rev.*, **106**, 1735-1741.

Madden, R., 1978: Further evidence of traveling planetary waves, *J. Atmos. Sci.*, **35**, 1605-1618.

Matsuno, T., 1971: A dynamic model of the stratospheric sudden warming, *J. Atmos. Sci.*, **28**, 1479-1492.

McGuirk, J.P., 1978: Planetary scale forcing of January 1977 weather, *Science*, **199**, 293-295.

Quiroz, R.S.: 1977, The tropospheric-stratospheric polar vortex breakdown of January 1977, *Geophys. Res. Lett.*, **4**, 151-154.

Ramanathan, V., 1977: Troposphere-stratospheric feedback mechanism: stratospheric warming and its effect on the polar energy budget and the tropospheric circulation, *J. Atmos. Sci.*, **34**, 439-447.

Schoeberl, M.R., 1978: Stratospheric warmings: Observation and theory, *Rev. of Geophys. and Space Phys.*, **16**, 521-538.

Schoeberl, M.R. and M.A. Geller, 1977: A calculation of the structure of stationary planetary waves in winter. *J. Atmos. Sci.*, **34**, 1235-1255.

Schoeberl, M.R. and D.F. Strobel: 1978a, The zonally averaged circulation of the middle atmosphere, *J. Atmos. Sci.*, **35**, 577-591.

Schoeberl, M.R. and D.F. Strobel, 1978b: The response of the zonally averaged circulation to stratospheric ozone reductions, *J. Atmos. Sci.*, **35**, 1751-1757.

Uryu, M., 1974: Mean zonal flows induced by vertically propagating Rossby wave packet, *J. Meteorol. Soc. Jap.*, **52**, 481-490.

van Loon, H., R.L. Jenne, and K. Labitzke, 1973: Zonal harmonic standing waves. *J. Geophys. Res.*, **78**, 4463-4471.

Table 1 — Summary of Warming Experiments

Experiment	m	$\bar{T}$			ϕ' (60°N)			$\bar{u}$	Integration Length	Description
		Max (K)	Alt (km)	Day	Max prewarming (dam)	Alt	Day	Initial Maximum	(days)	(Section)
Undamped	1	32	65	016	230	70	20	71	040	3
Warming		47	60	024	210	68	26			
Isothermal		47	28	026	240	65	32			
Damped	1	07	60	17	145	70	13	87	120	4
Warming		06	60	027	125	30	27			
Isothermal		22	30	050	070	40	37			
Damped	1	06	60	016	150	70	14	87	060	5
Warming		22	30	045	110	70	27			
Nonisothermal,					080	35	24			
Damped	1	03	60	015	126	70	15	87	060	5
M = 0 warming		06	25	030	055	70	46			
Undamped	2	73	36	025	110	75	24	71	040	3
Warming		75	65	027	115	42	22			
Damped	2	42	30	044	096	45	37	87	180	4
Warming		33	30	110						
		30	30	168						
Nonisothermal, Damped	2	50	27	040	085	40	32	87	060	5
M = 0 Damped	2	12	25	042	032	20	22	87	060	5
Damped Isothermal	3	05	25	060	030	18	40	87	060	5

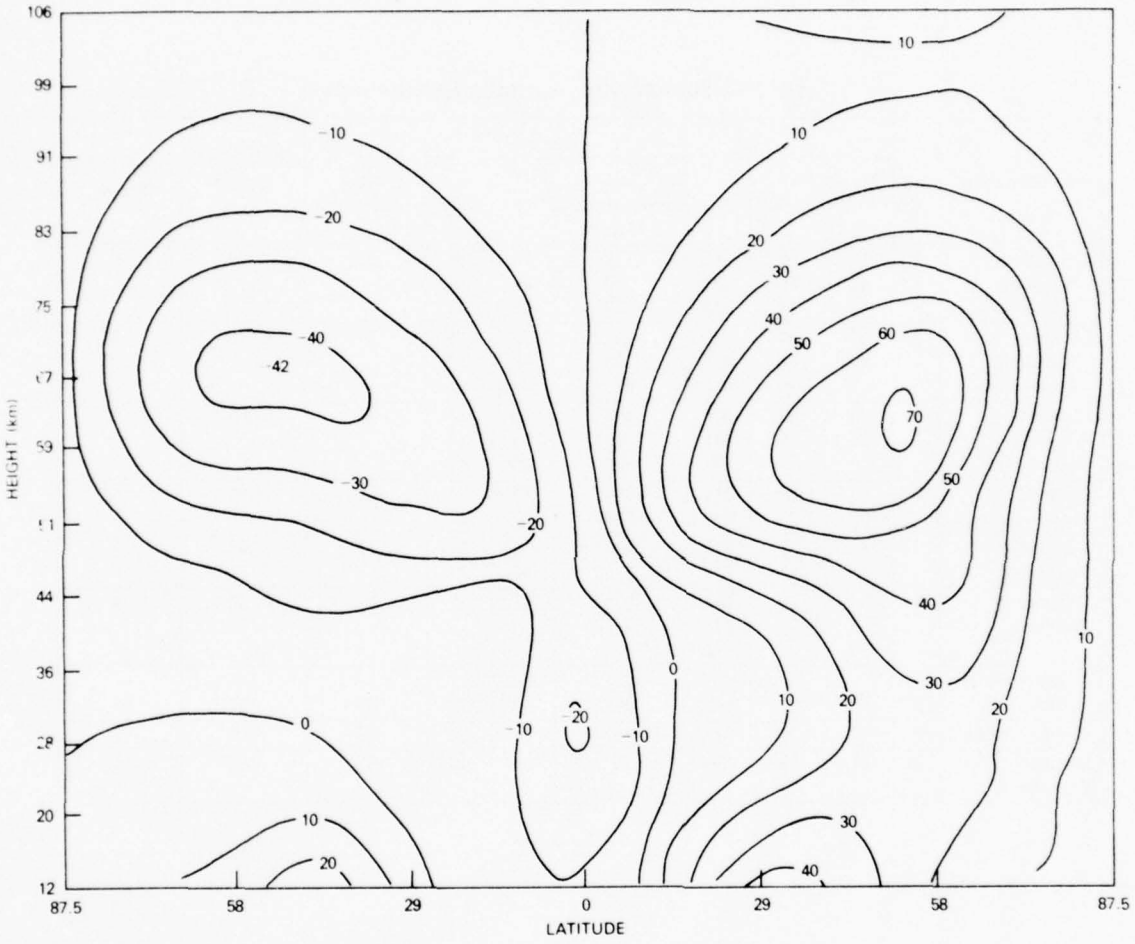

(a)

Fig. 1 — The mean zonal wind models used in this study. Part a shows the weak polar night jet model for simulations with no damping. Part b, the wind model from Paper I with a momentum source, M, for the lower stratosphere. Part c, same as part b but M set to zero. The indicated height is the globally averaged height of the pressure field.

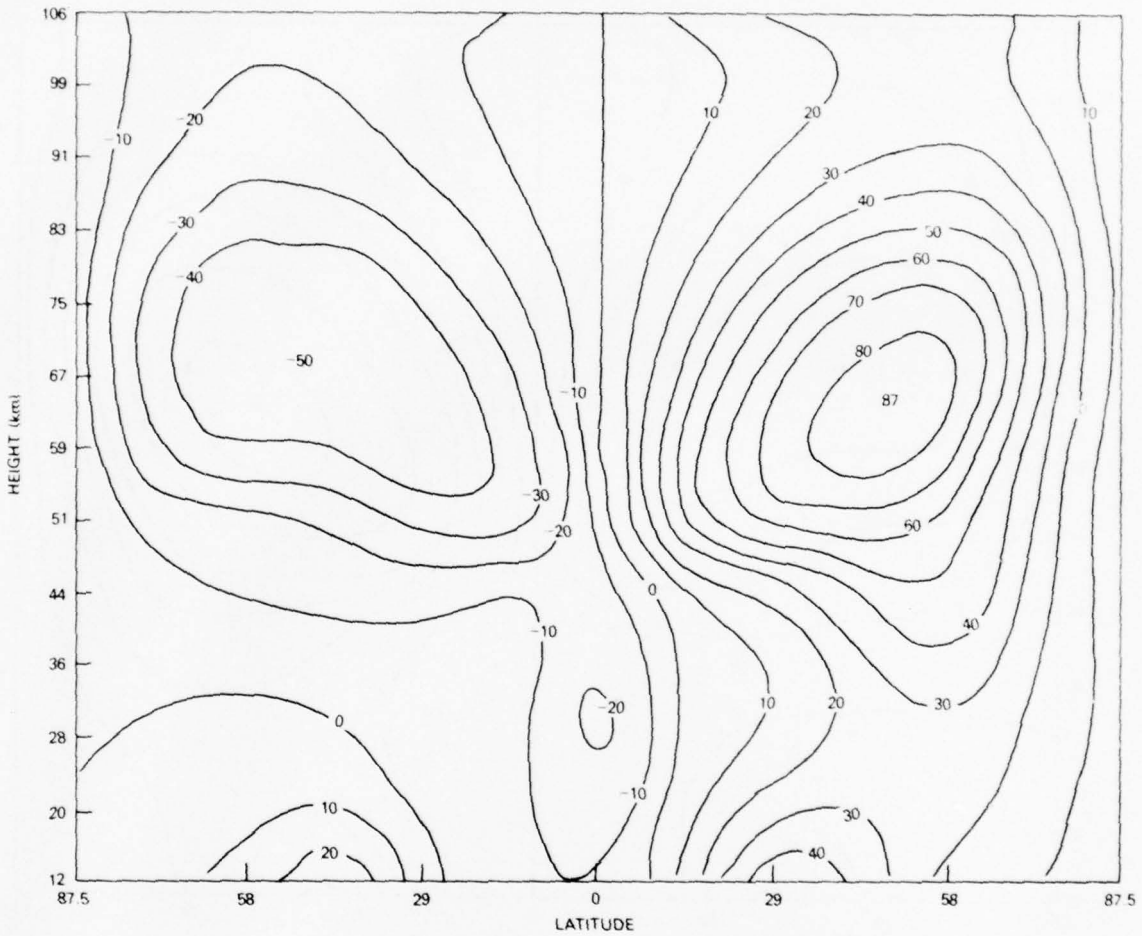

(c)

Fig. 1 (Continued) — The mean zonal wind models used in this study. Part a shows the weak polar night jet model for simulations with no damping. Part b, the wind model from Paper I with a momentum source, M, for the lower stratosphere. Part c, same as part b but M set to zero. The indicated height is the globally averaged height of the pressure field.

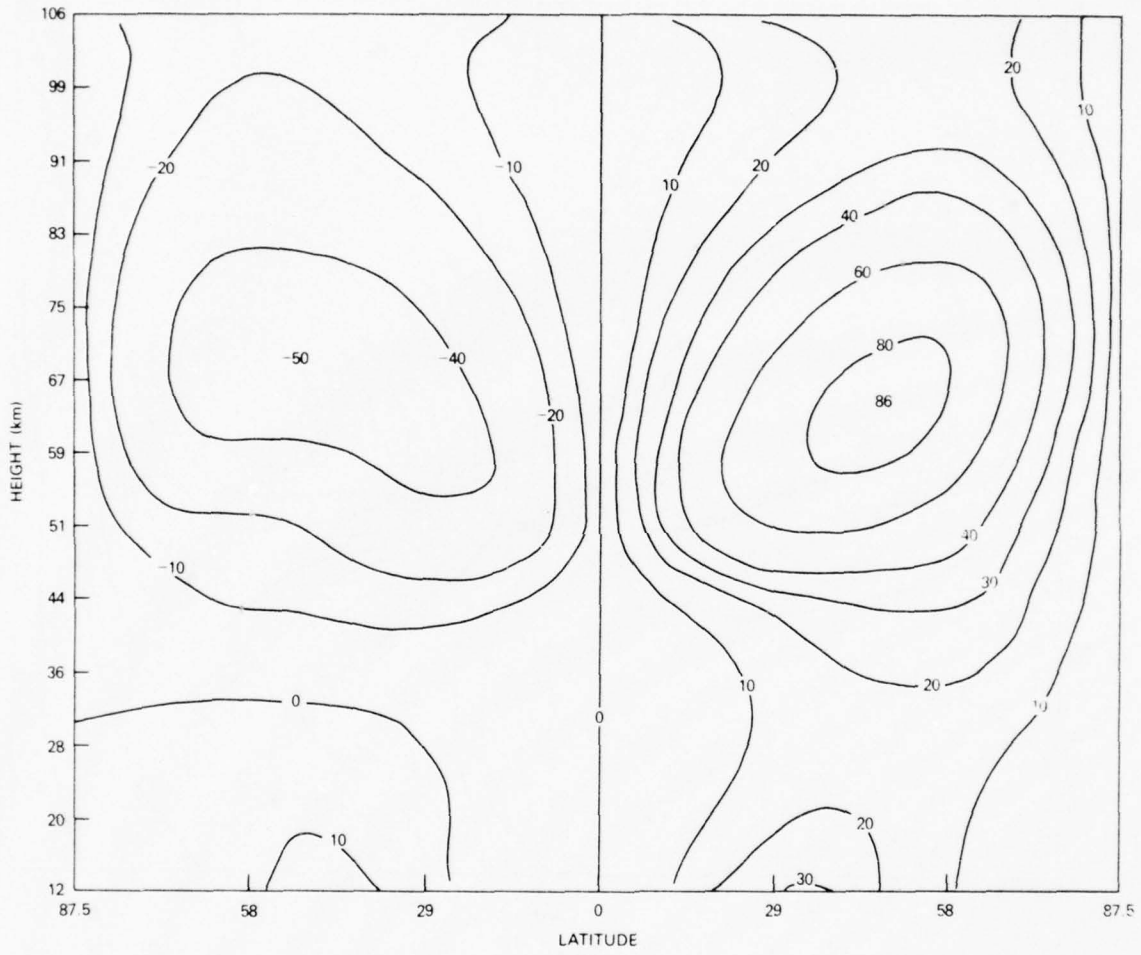

(c)

Fig. 1 (Continued) — The mean zonal wind models used in this study. Part a shows the weak polar night jet model for simulations with no damping. Part b, the wind model from Paper I with a momentum source, M, for the lower stratosphere. Part c, same as part b but M set to zero. The indicated height is the globally averaged height of the pressure field.

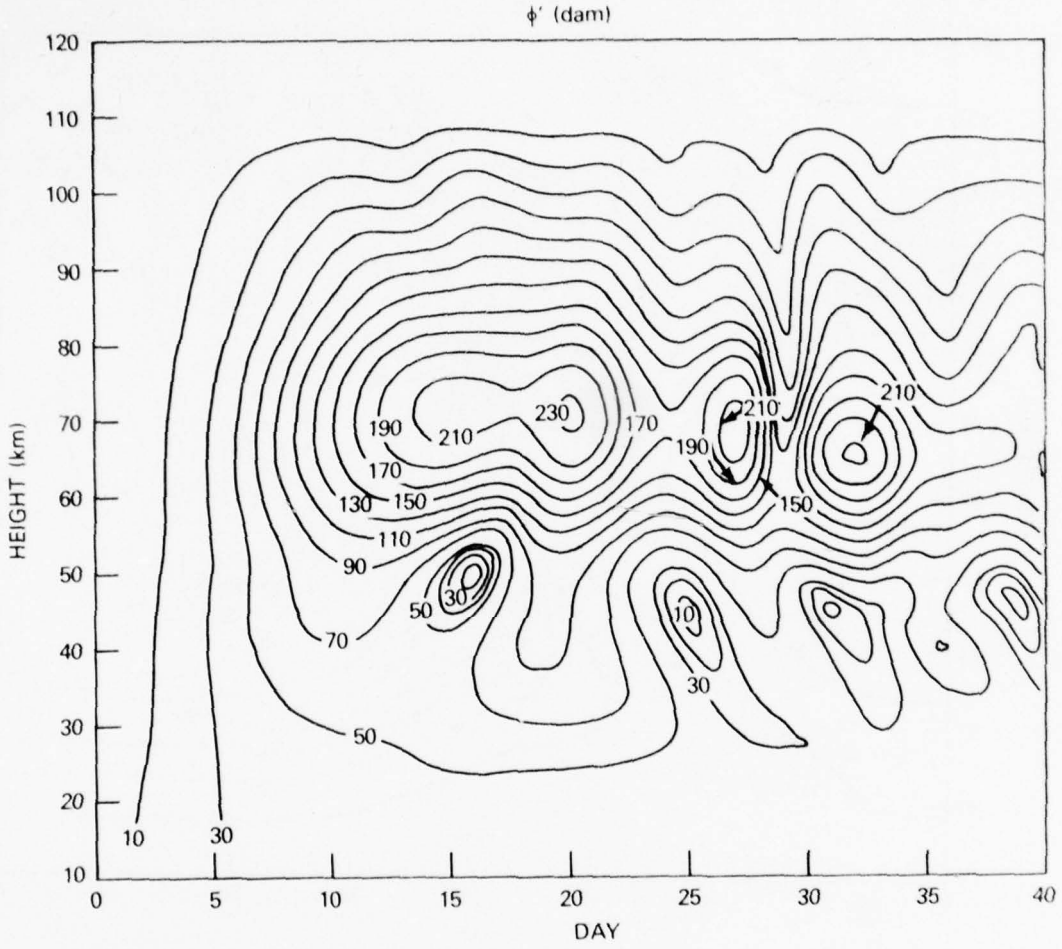

a)

Fig. 2 — Constant contours of ϕ' at (60)°N (part a) with 10 dam intervals; u at 57.5°N (part b) with 10 ms^{-1} intervals; ΔT at 87.5°N (part c) with 5 K intervals, and T' at 60°N (part b) with 5K intervals as a function of height and time for $m = 1$, undamped warming. $\Delta T = T(t) - T(0)$.

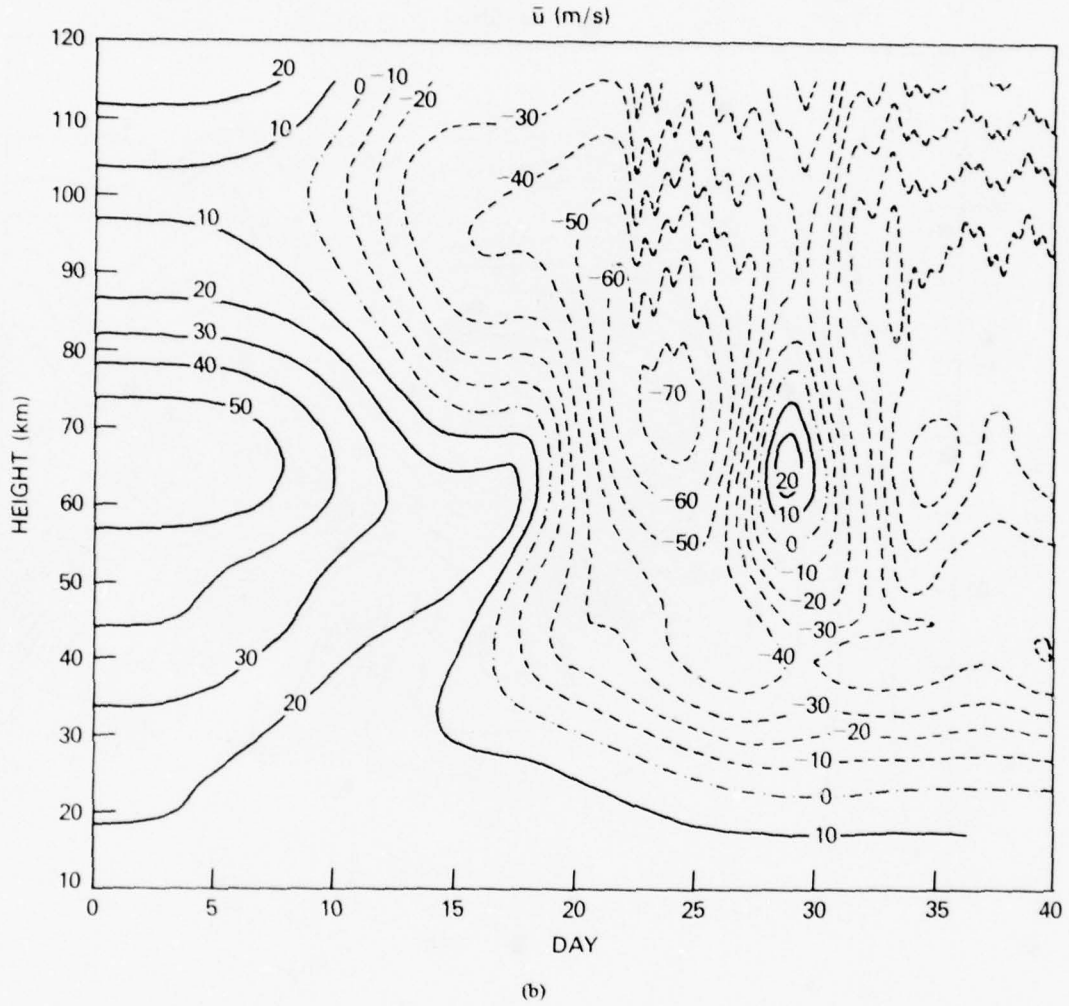

(b)

Fig. 2 (Continued) — Constant contours of ϕ' at (60)°N (part a) with 10 dam intervals; u at 57.5°N (part b) with 10 ms^{-1} intervals; ΔT at 87.5°N (part c) with 5 K intervals, and T' at 60°N (part b) with 5K intervals as a function of height and time for $m = 1$, undamped warming. $\Delta T = T(t) - T(0)$.

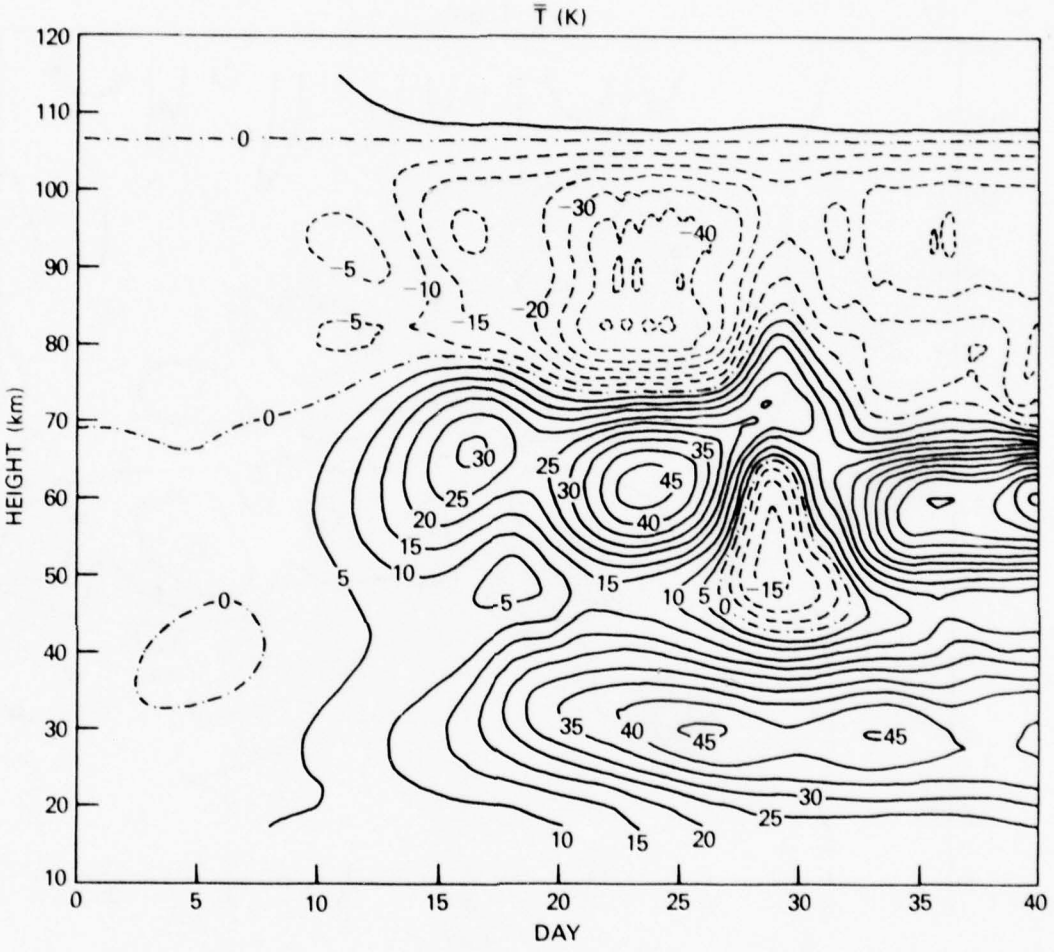

(c)

Fig. 2 (Continued) — Constant contours of ϕ at (60)°N (part a) with 10 dam intervals; u at 57.5°N (part b) with 10 ms^{-1} intervals; ΔT at 87.5°N (part c) with 5 K intervals, and $\bar{T}$ at 60°N (part b) with 5K intervals as a function of height and time for $m = 1$, undamped warming. $\Delta T = T(t) - T(0)$.

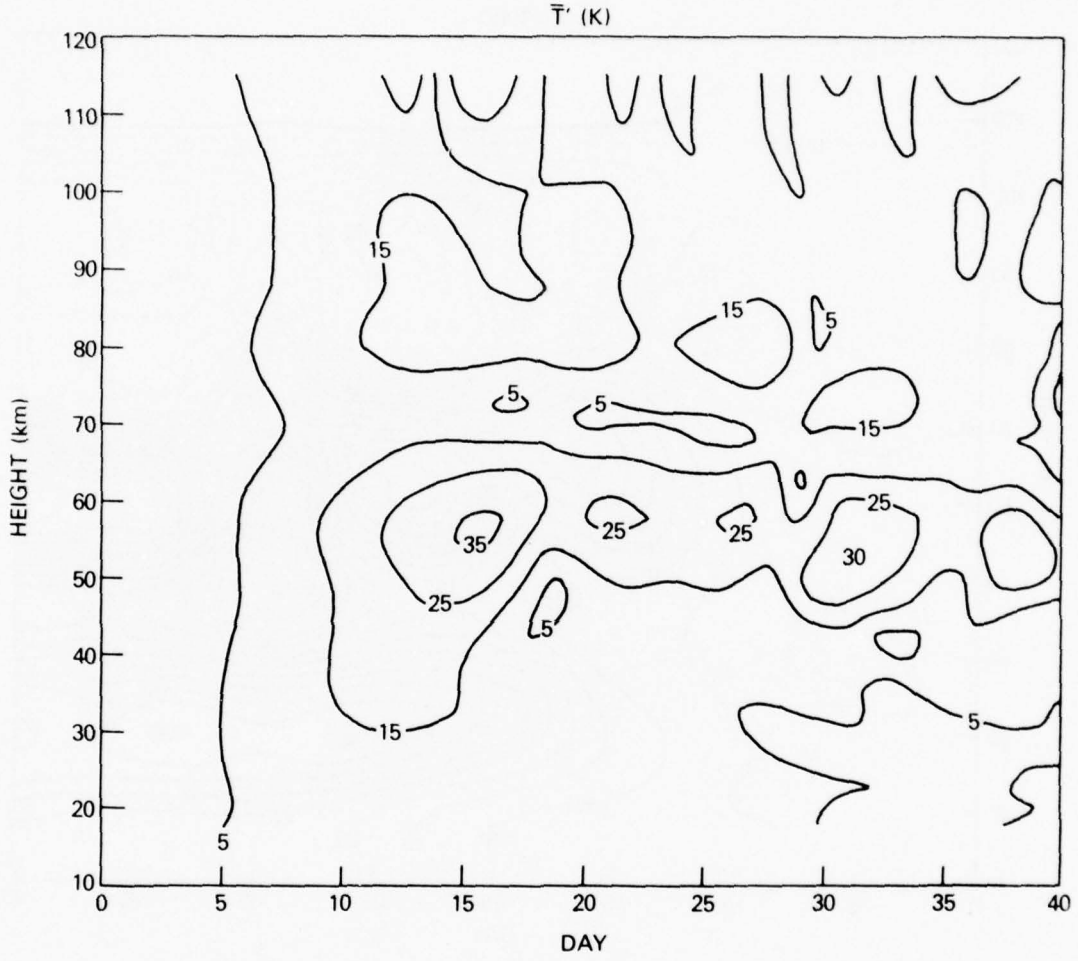

(d)

Fig. 2 (Continued) — Constant contours of ϕ' at (60)°N (part a) with 10 dam intervals; u at 57.5°N (part b) with 10 ms^{-1} intervals; ΔT at 87.5°N (part c) with 5 K intervals, and T' at 60°N (part b) with 5K intervals as a function of height and time for $m = 1$, undamped warming. $\Delta T = \bar{T}(t) - \bar{T}(0)$.

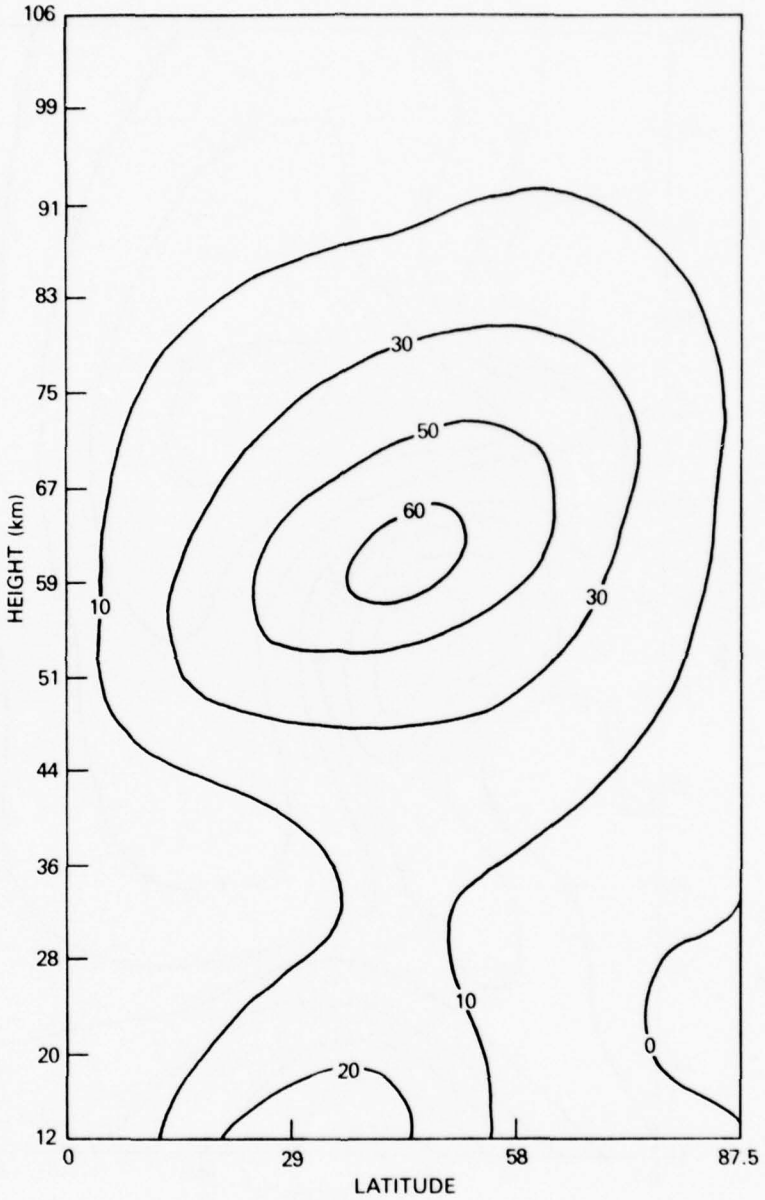

(a)

Fig. 3 — The mean zonal wind in the winter hemisphere at day 10 (part a) and day 25 (part b) corresponding to Fig. 2b.

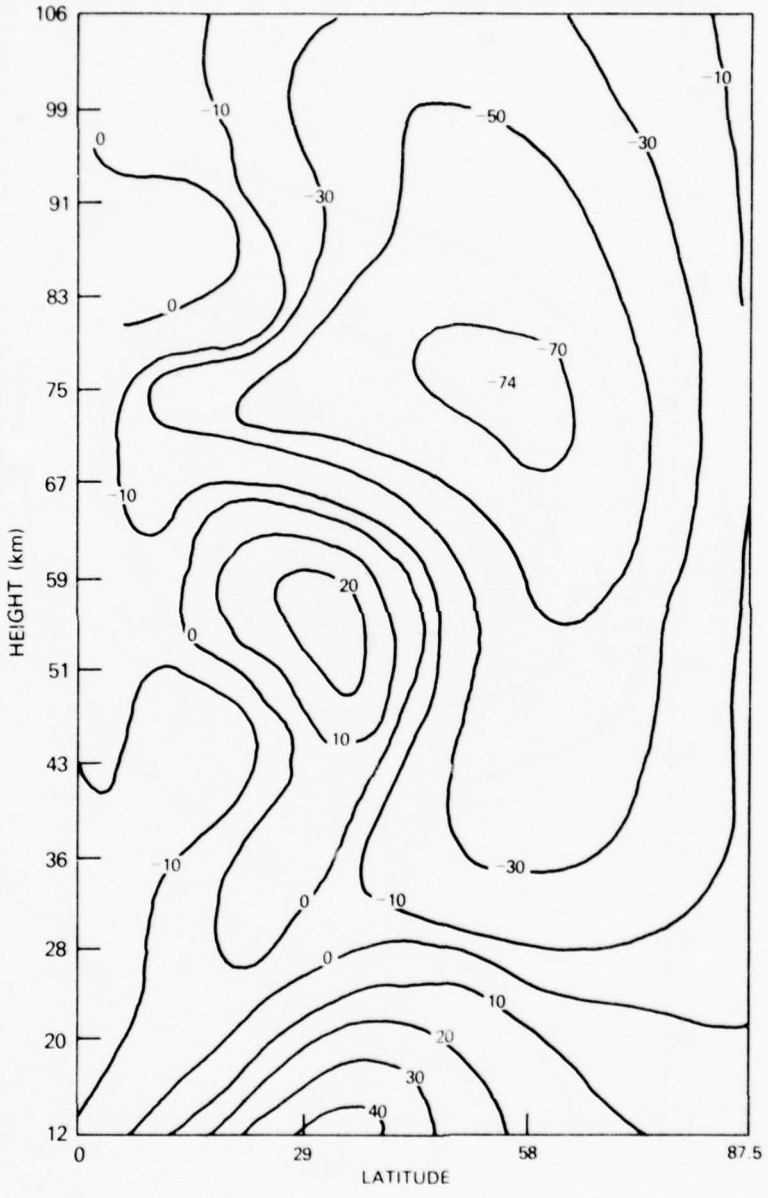

(b)

Fig. 3 (Continued) — The mean zonal wind in the winter hemisphere at day 10 (part a) and day 25 (part b) corresponding to Fig. 2b.

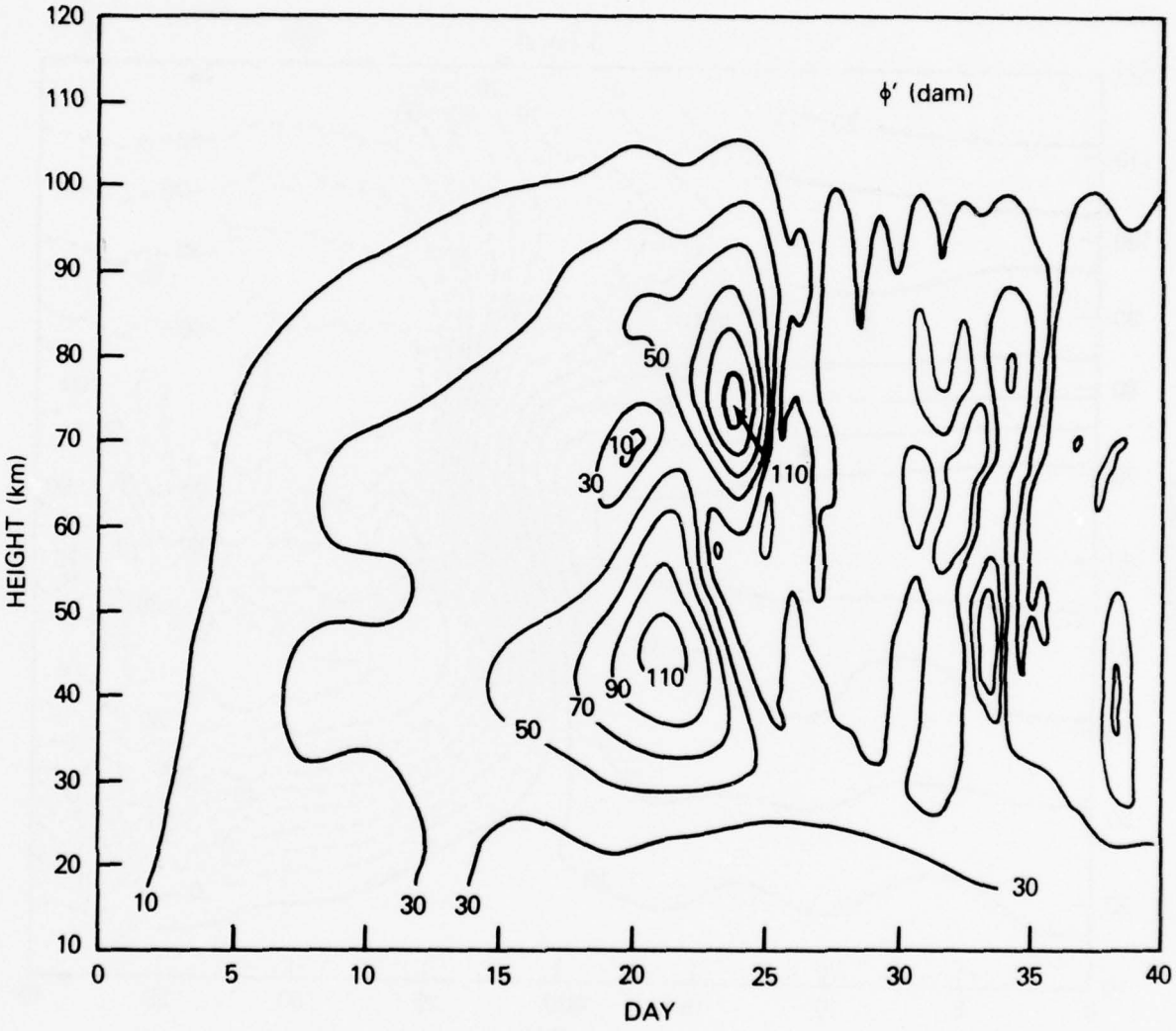

(a)

Fig. 4 — Same as Fig. 2 but $m = 2$, no damping.

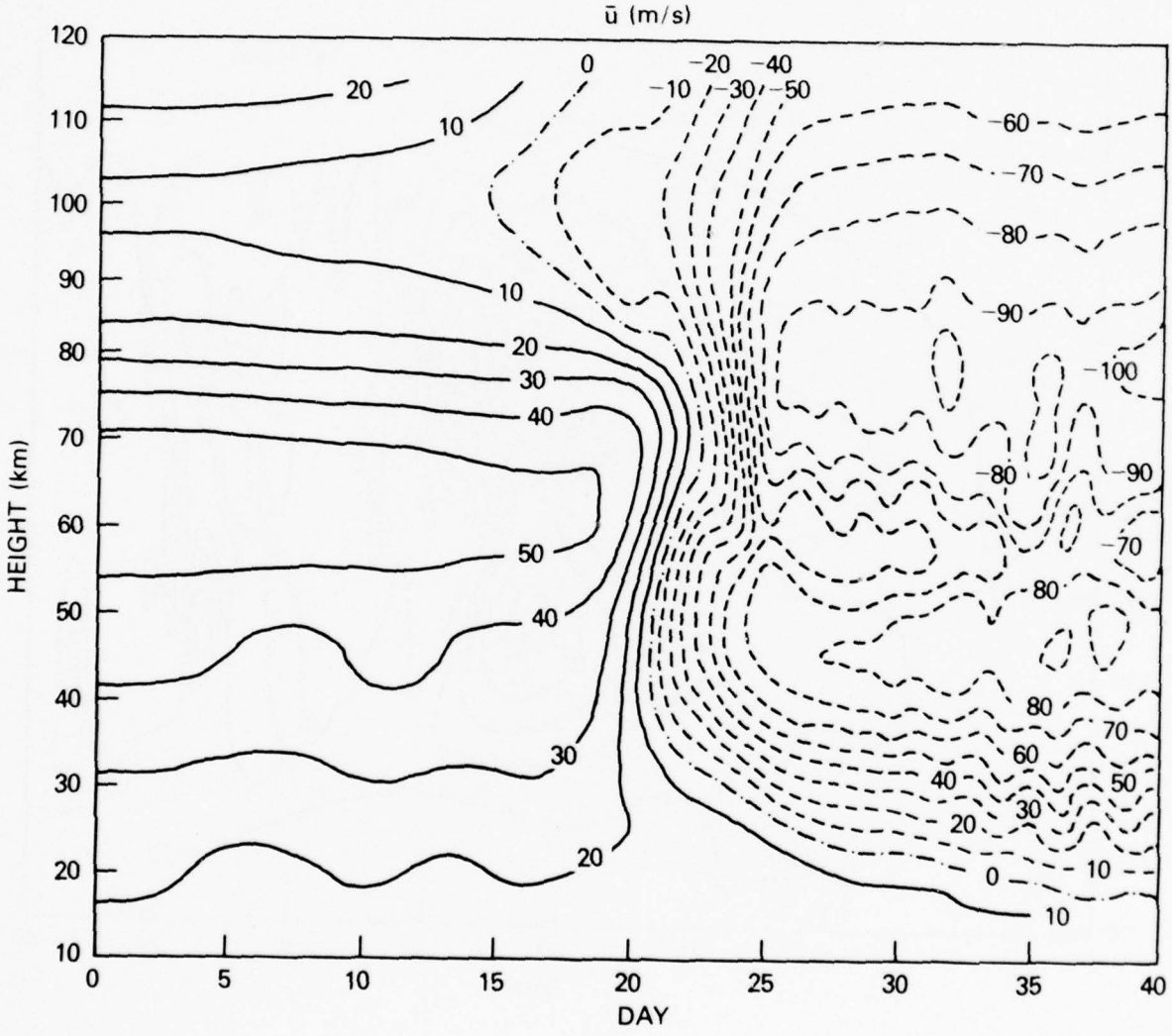

(b)

Fig. 4 (Continued) — Same as Fig. 2 but $m = 2$, no damping.

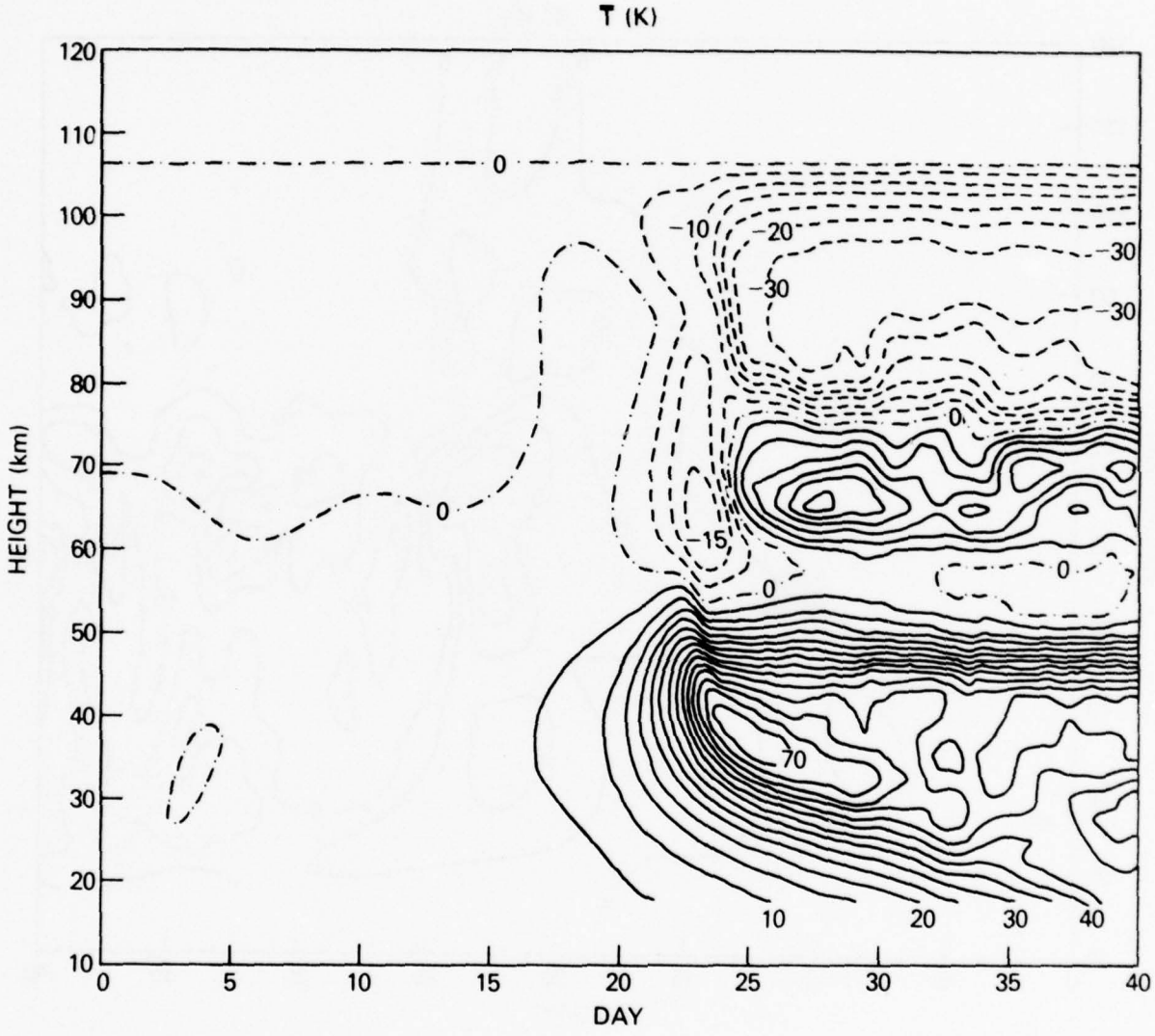

(c)

Fig. 4 (Continued) — Same as Fig. 2 but $m = 2$, no damping.

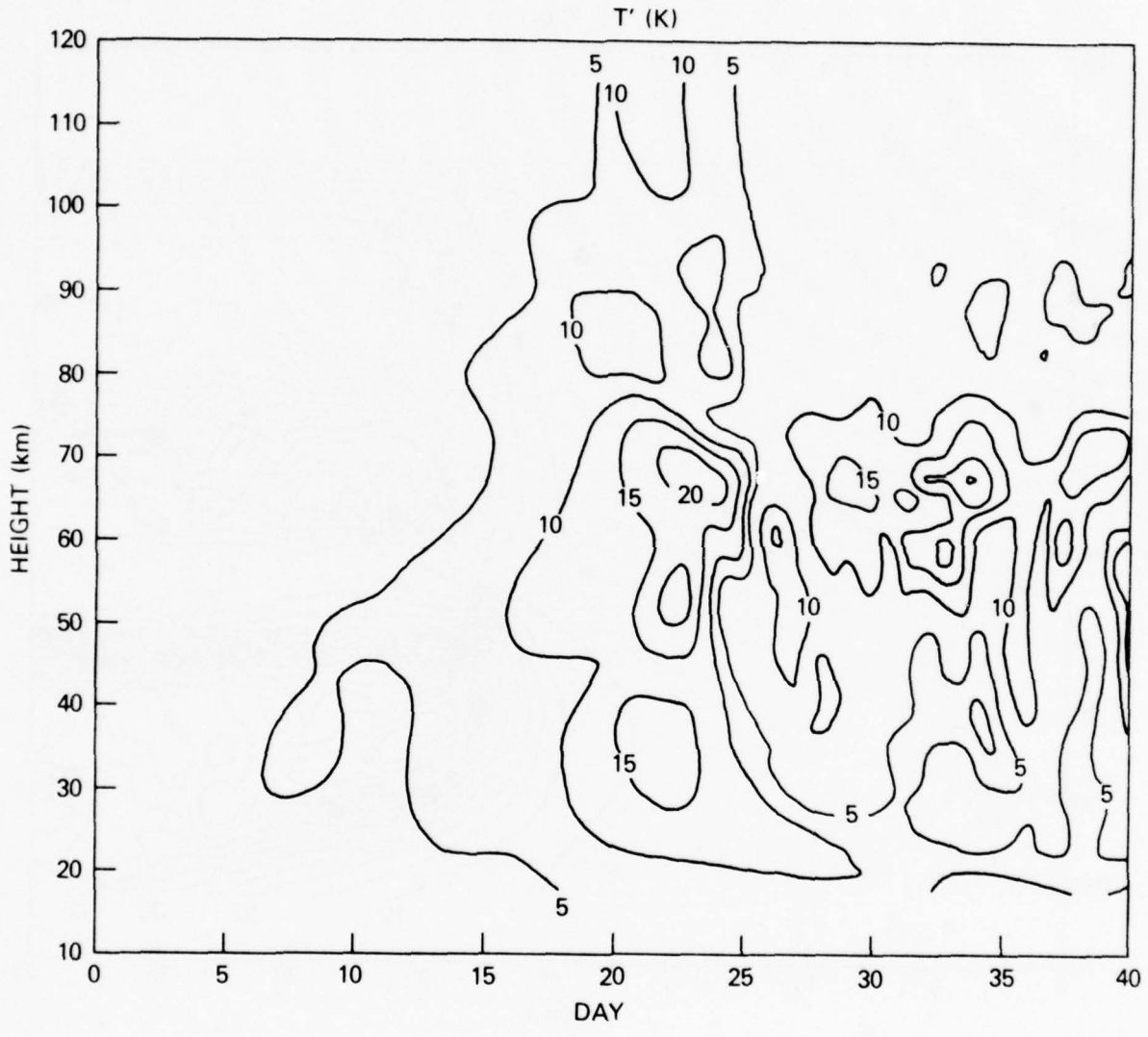

(d)

Fig. 4 (Continued) — Same as Fig. 2 but $m = 2$, no damping.

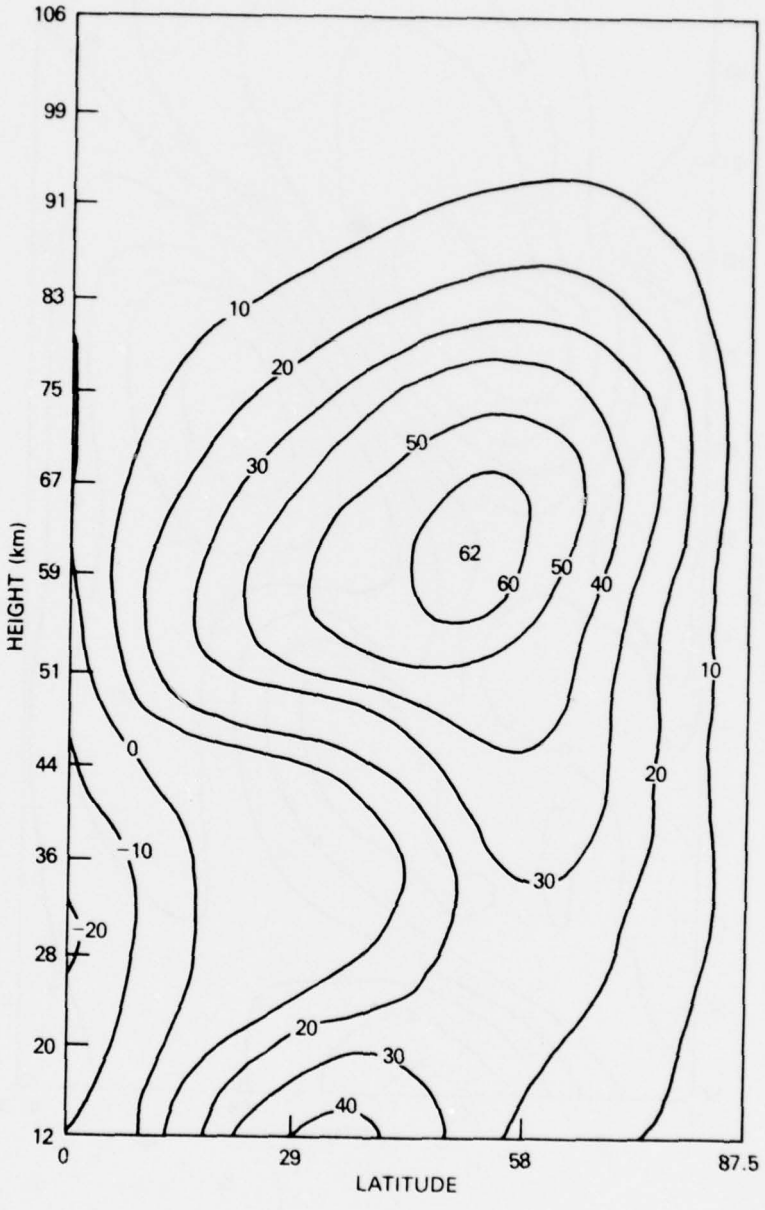

(a)

Fig. 5 — Same as Fig. 3 but $m = 2$, no damping; (a) day 10, (b) day 20, (c) day 25.

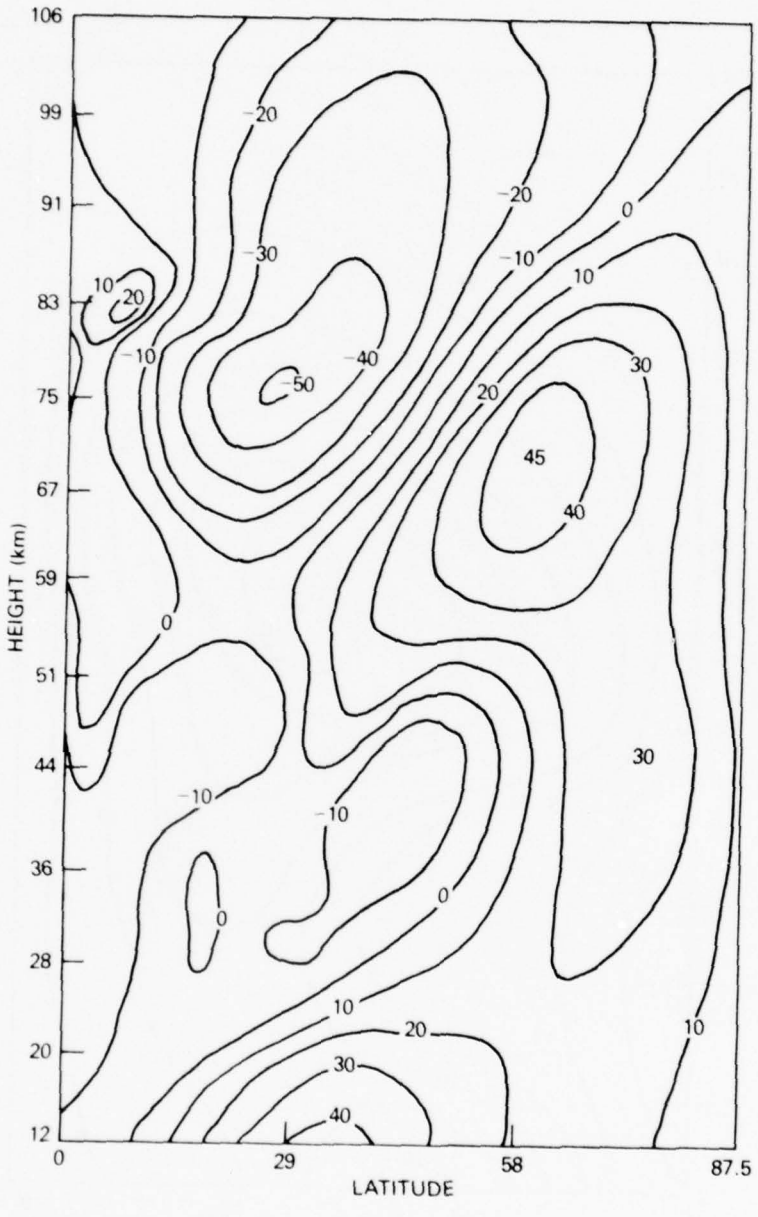

(b)

Fig. 5 (Continued) — Same as Fig. 3 but $m = 2$, no damping; (a) day 10, (b) day 20, (c) day 25.

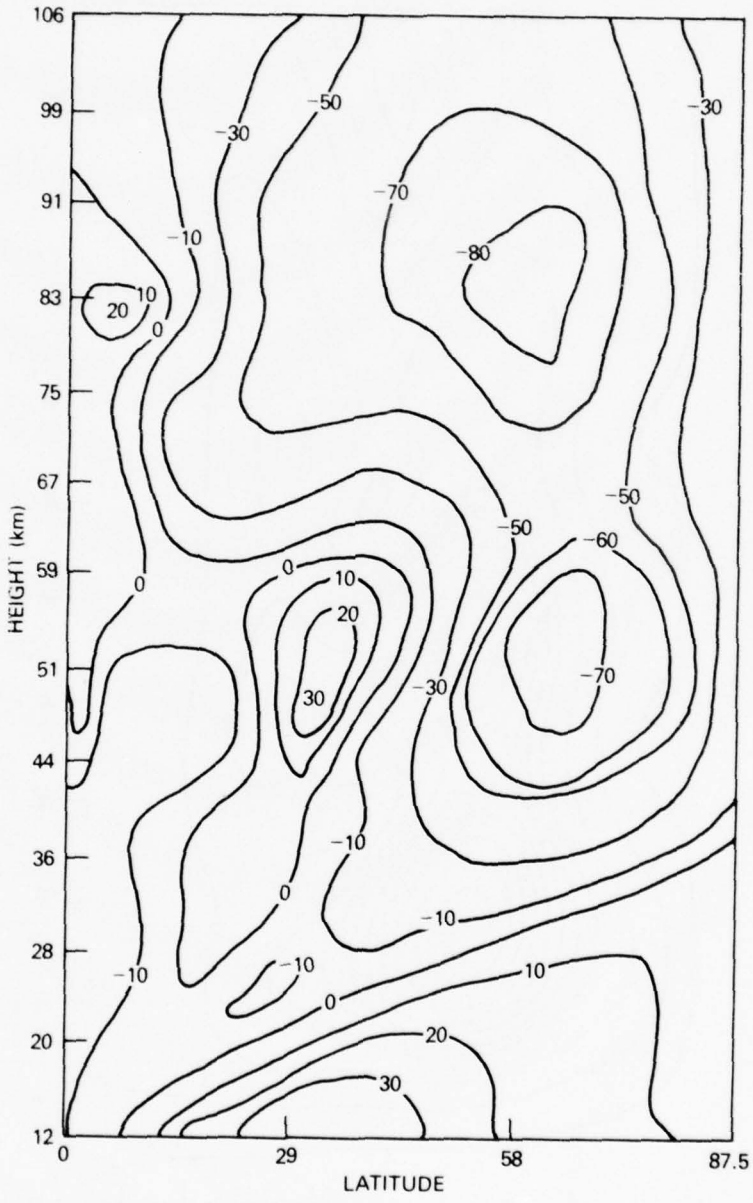

(c)

Fig. 5 (Continued) — Same as Fig. 3 but $m = 2$, no damping, (a) day 10, (b) day 20, (c) day 25.

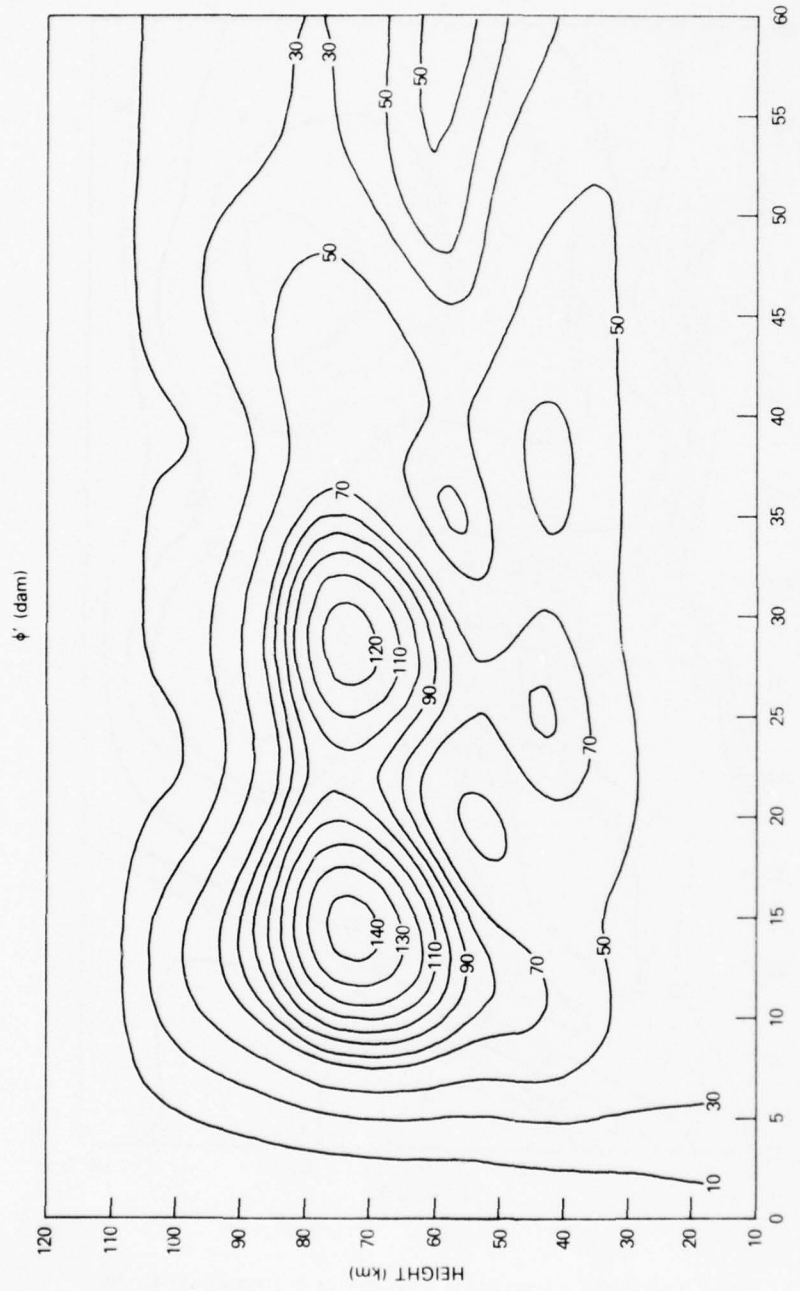

Fig. 6 — Same as Fig. 2 but $m = 1$, with damping.

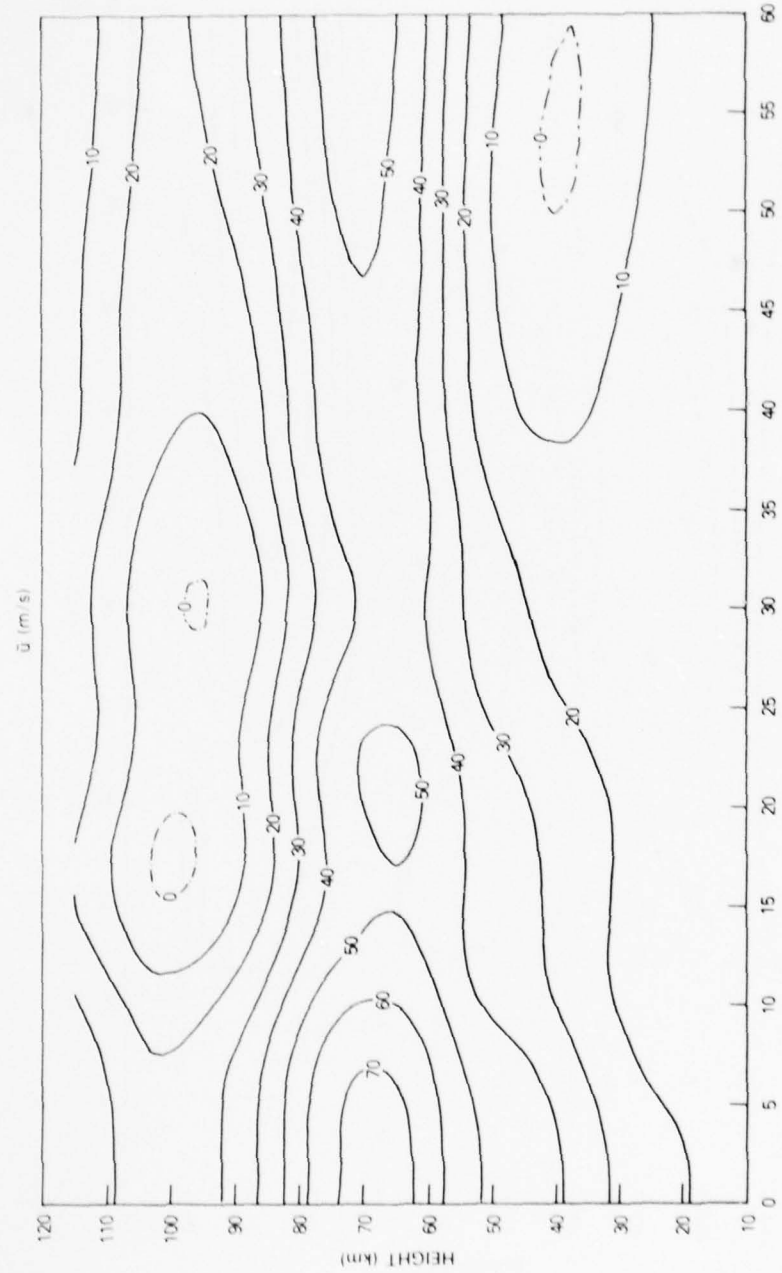

Fig. 6 (Continued) — Same as Fig. 2 but $m = 1$, with damping

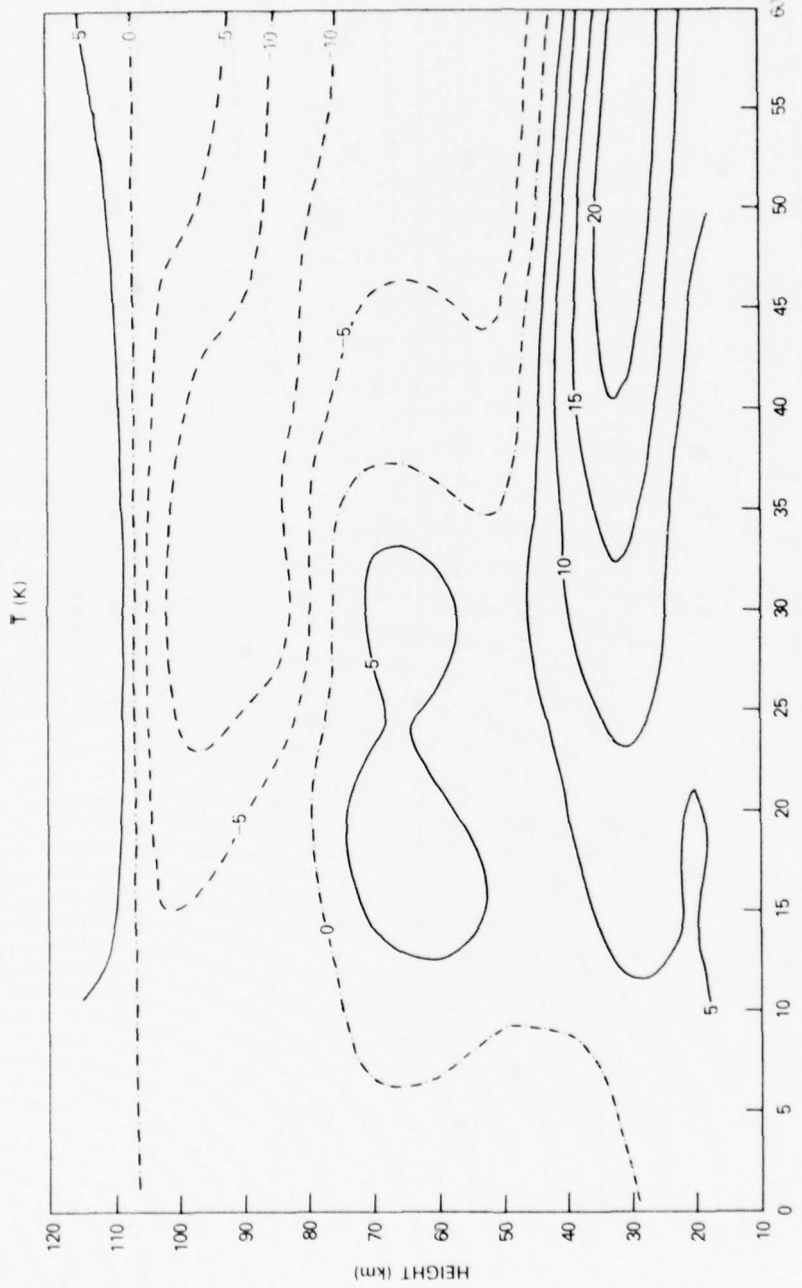

Fig. 6 (Continued) — Same as Fig. 2 but $m = 1$, with damping.

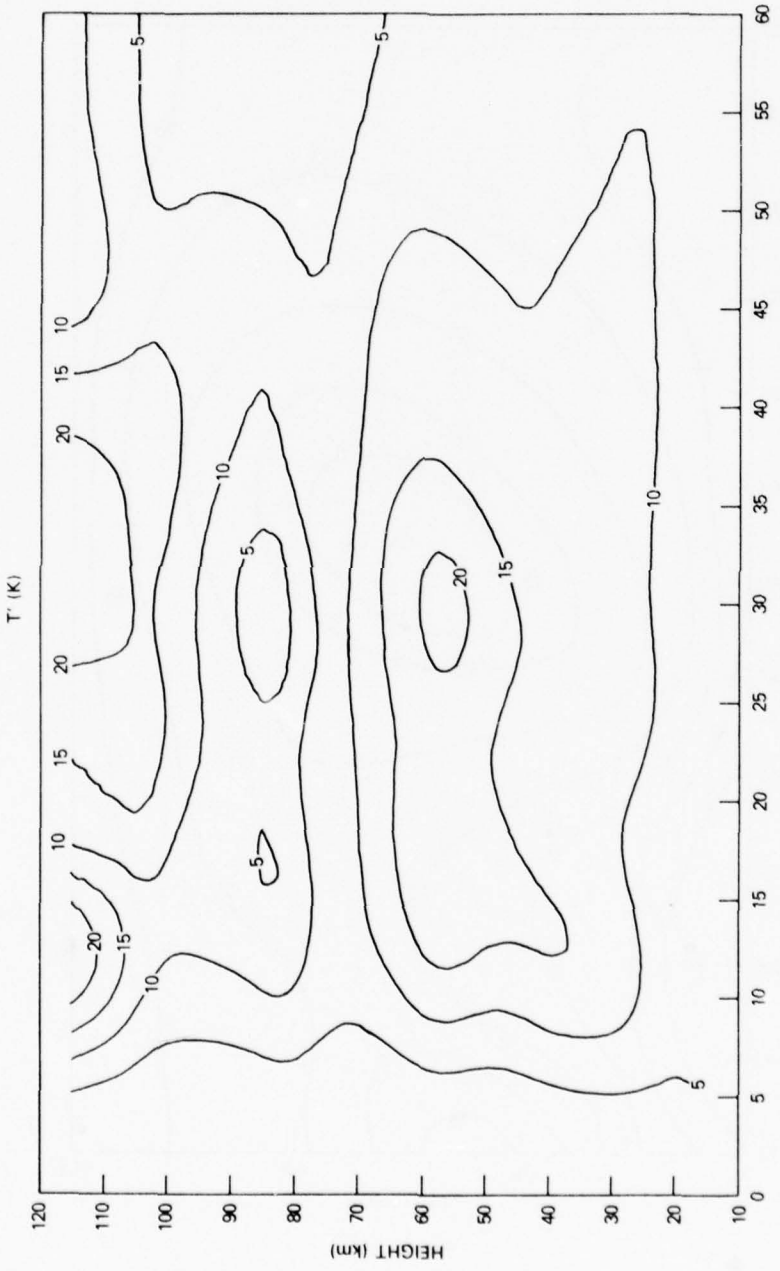

Fig. 6 (Continued) — Same as Fig. 2 but $m = 1$, with damping

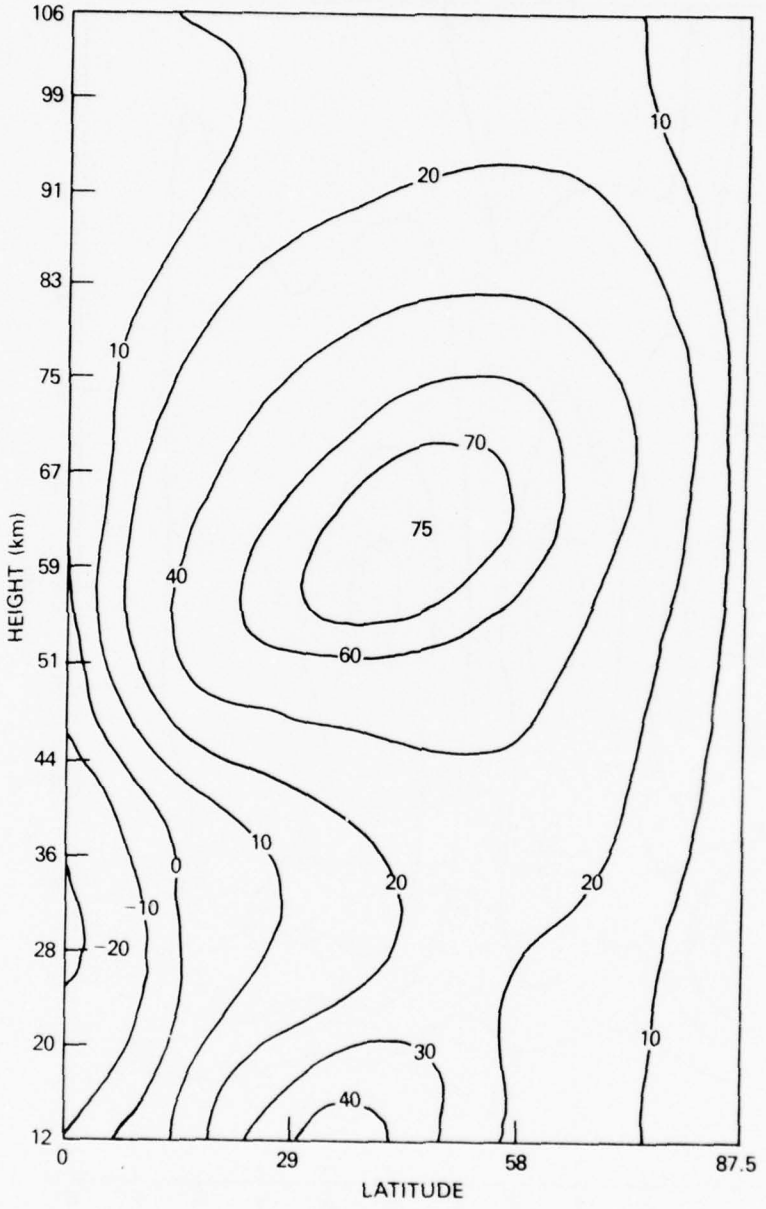

(a)

Fig. 7 — Same as Fig. 3 but $m = 1$, with damping; (a) day 10 (b) day 35, (c) day 45, (d) day 50, (e) day 55.

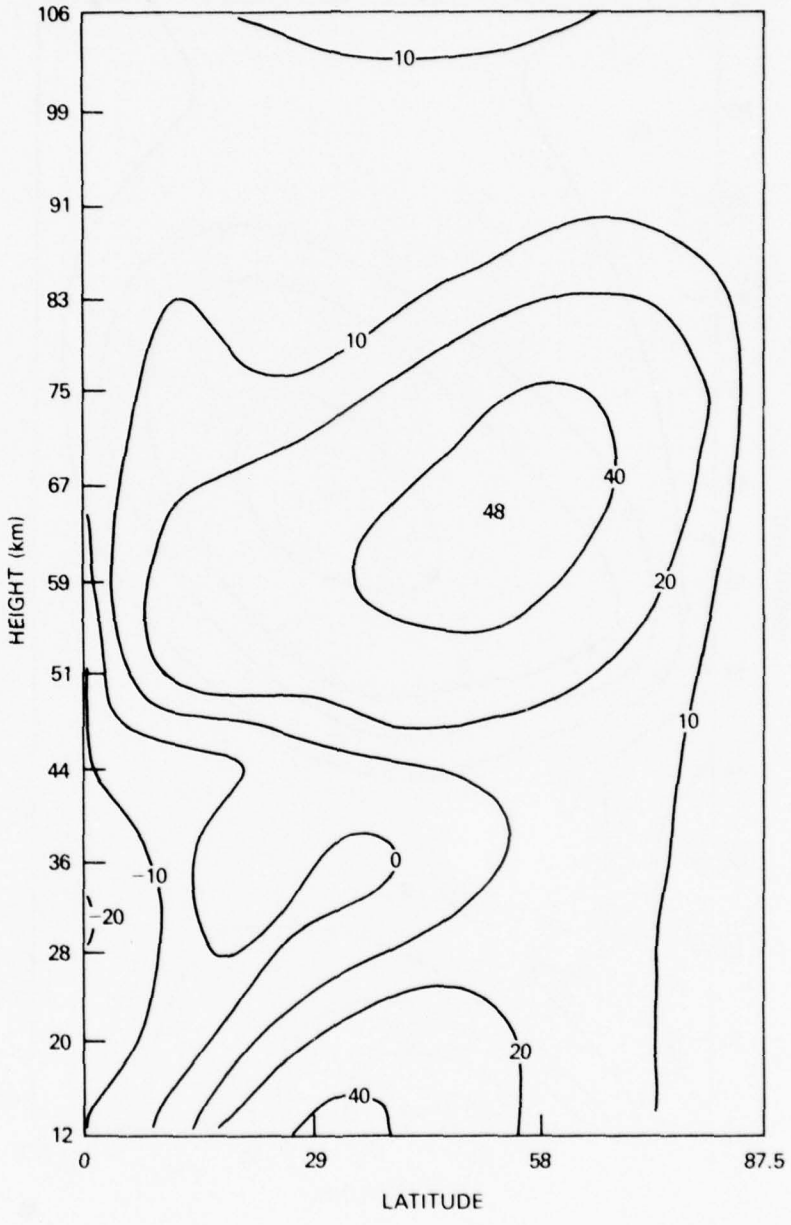

(b)

Fig. 7 (Continued) — Same as Fig. 3 but $m = 1$, with damping, (a) day 10 (b) day 35, (c) day 45, (d) day 50, (e) day 55.

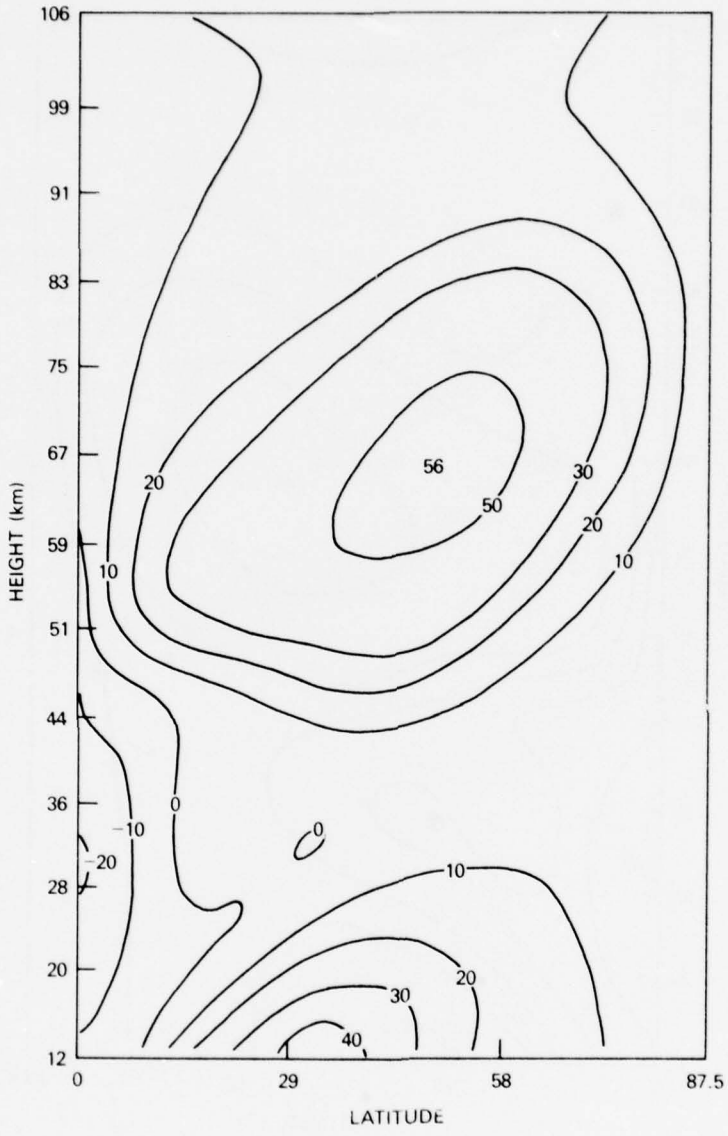

(c)

Fig. 7 (Continued) — Same as Fig. 3 but $m = 1$, with damping. (a) day 10 (b) day 35, (c) day 45, (d) day 50, (e) day 55.

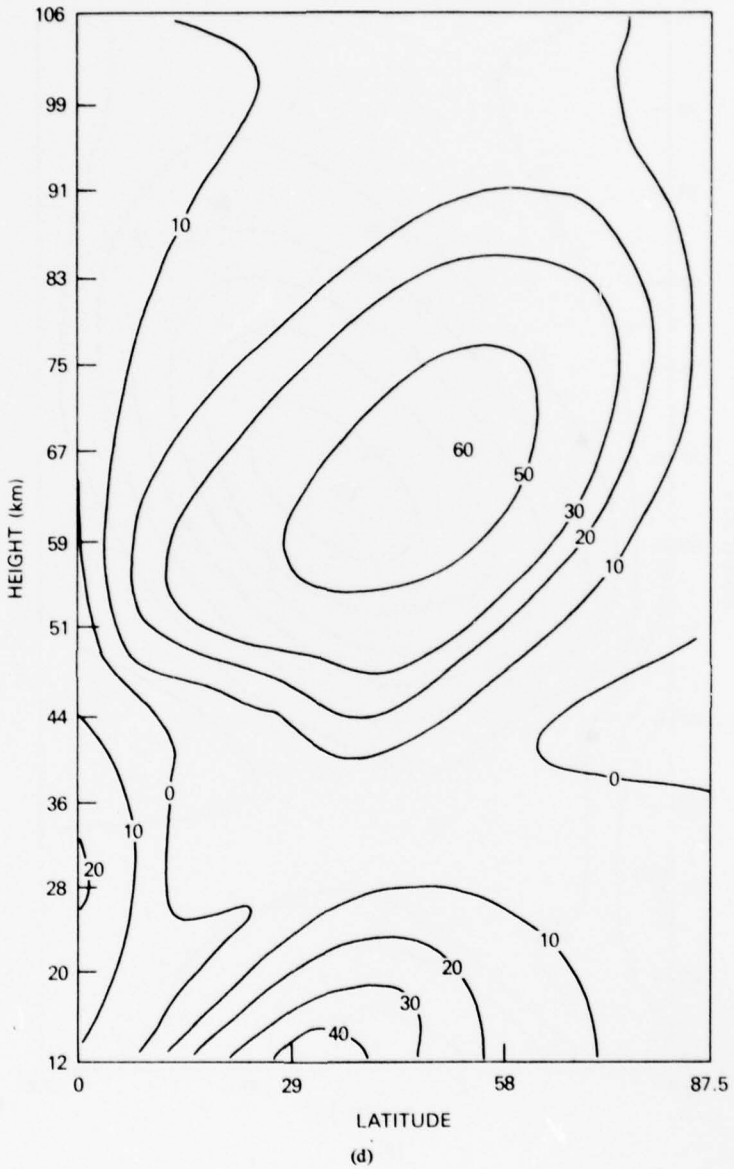

(d)

Fig. 7 (Continued) — Same as Fig. 3 but $m = 1$, with damping; (a) day 10 (b) day 35, (c) day 45, (d) day 50, (e) day 55.

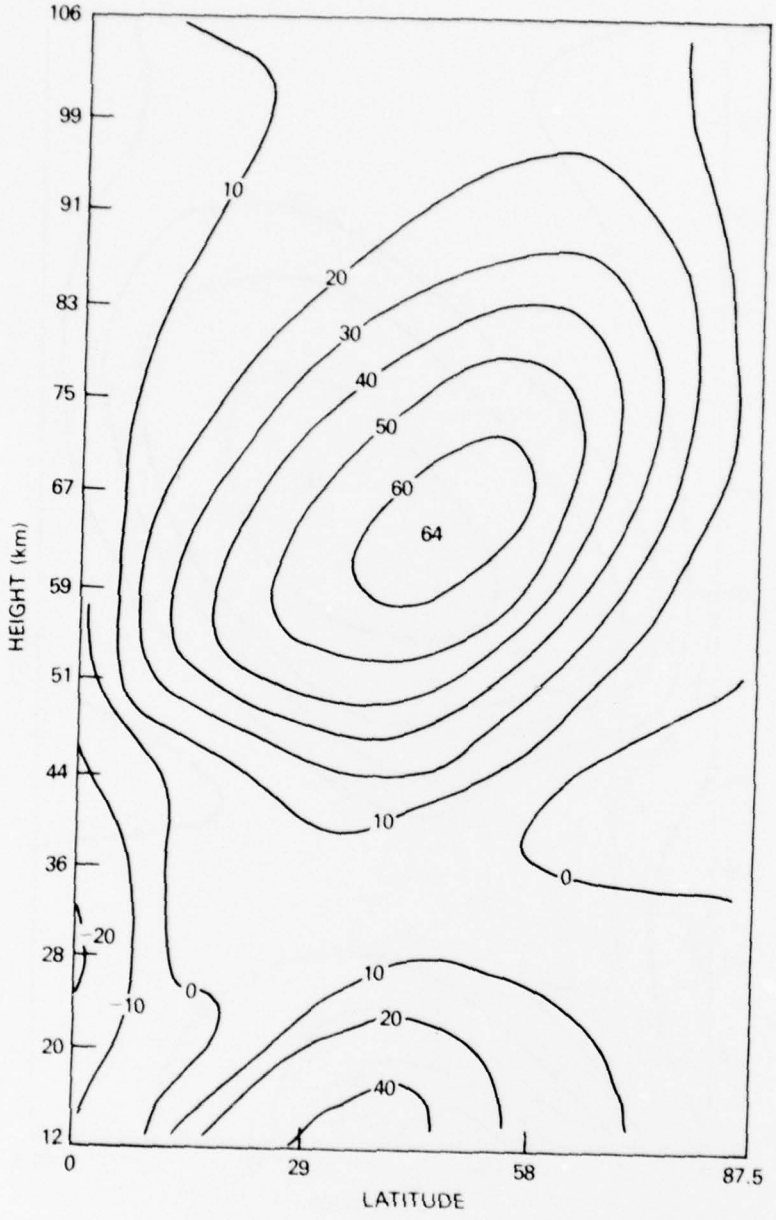

(e)

Fig. 7 (Continued) — Same as Fig. 3 but $m = 1$, with damping; (a) day 10 (b) day 35, (c) day 45, (d) day 50, (e) day 55.

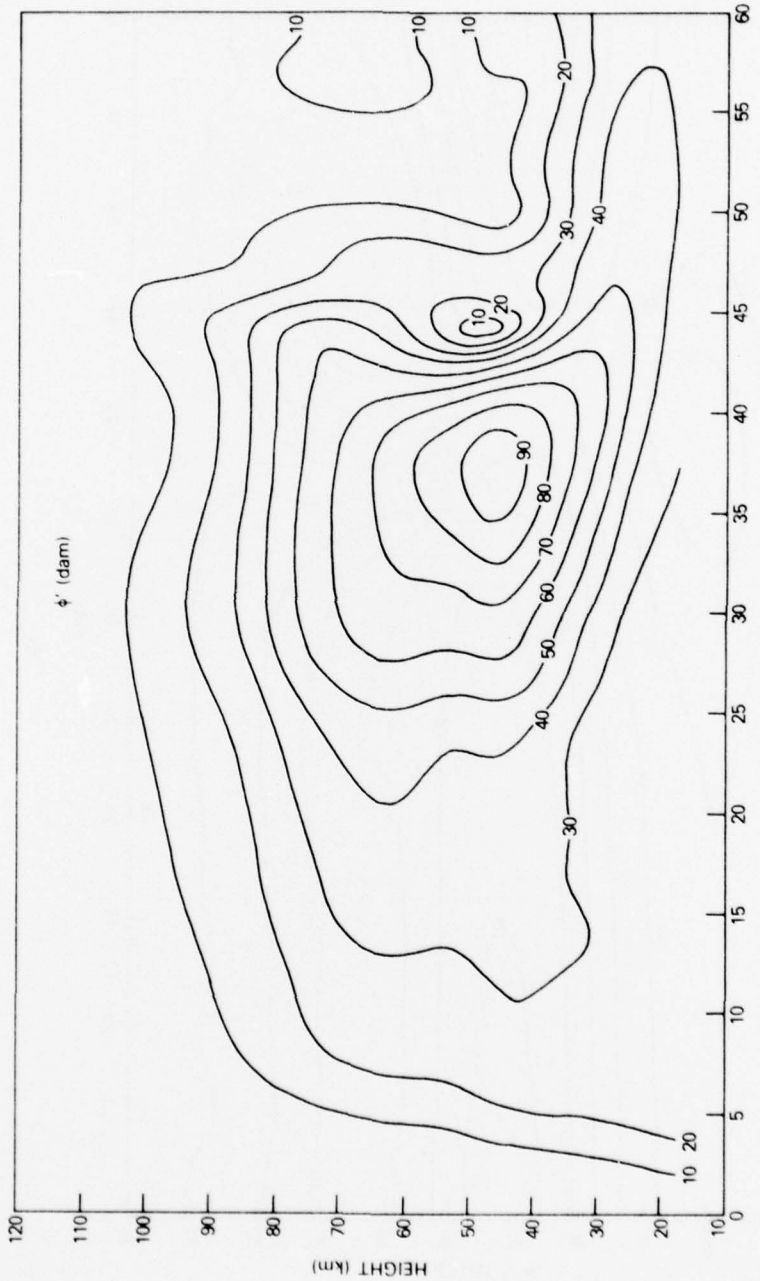

Fig. 8 — Same as Fig. 2 but $m = 2$, with damping.

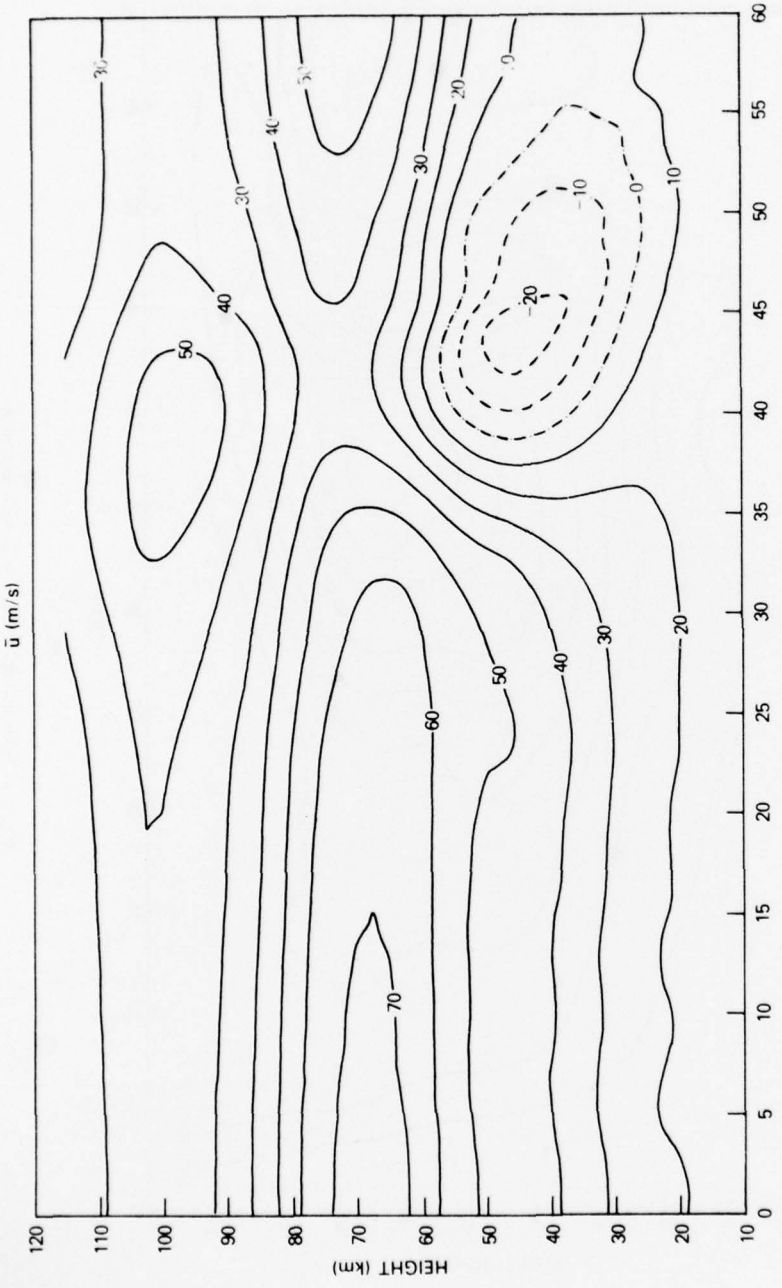

(b)

Fig. 8 (Continued) — Same as Fig. 2 but $m = 2$, with damping.

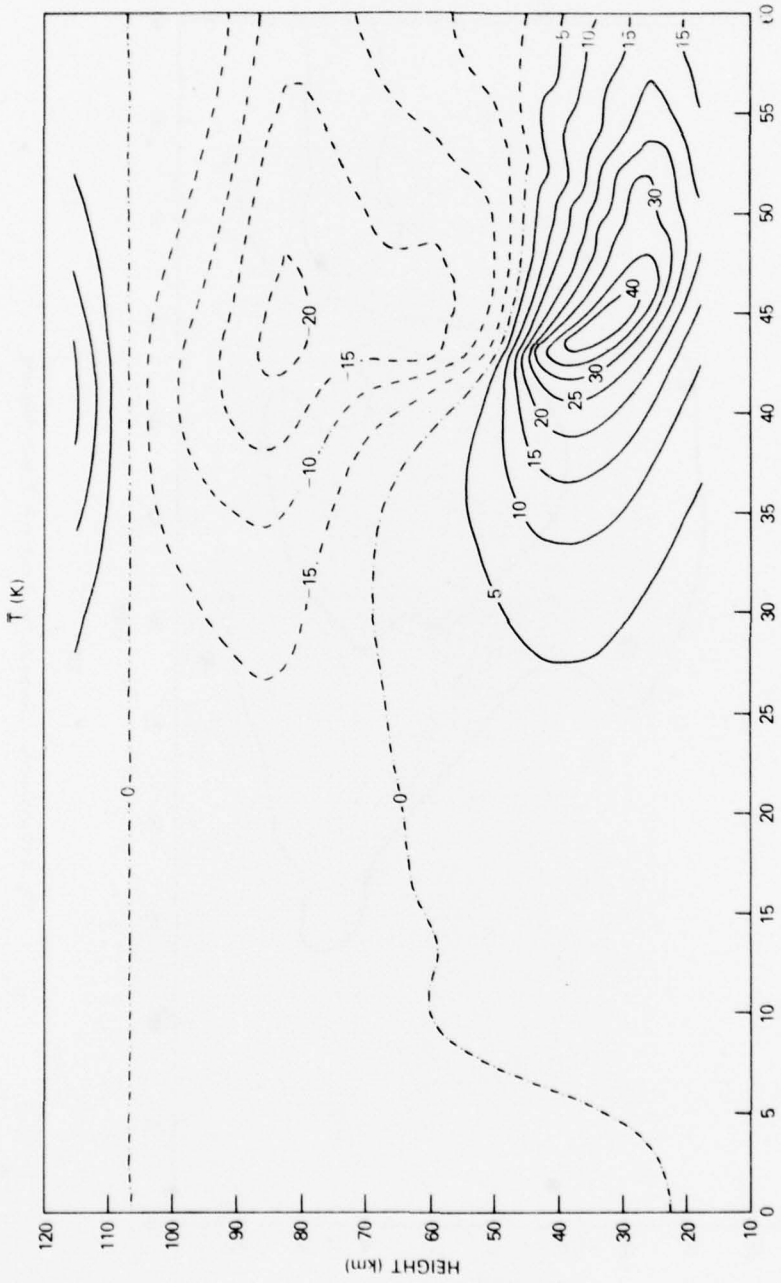

Fig. 8 (Continued) — Same as Fig. 2 but $m = 2$, with damping

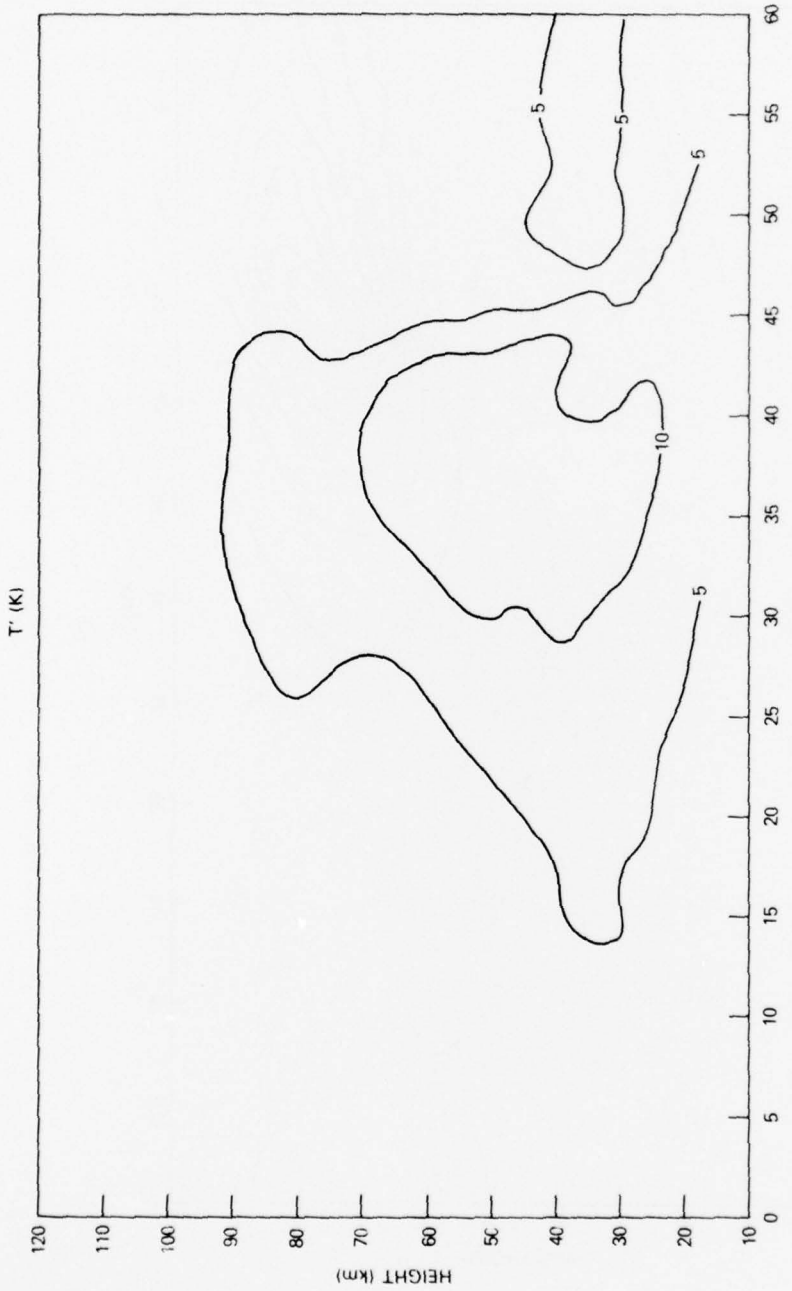

Fig. 8 (Continued) — Same as Fig. 2 but $m = 2$, with damping.

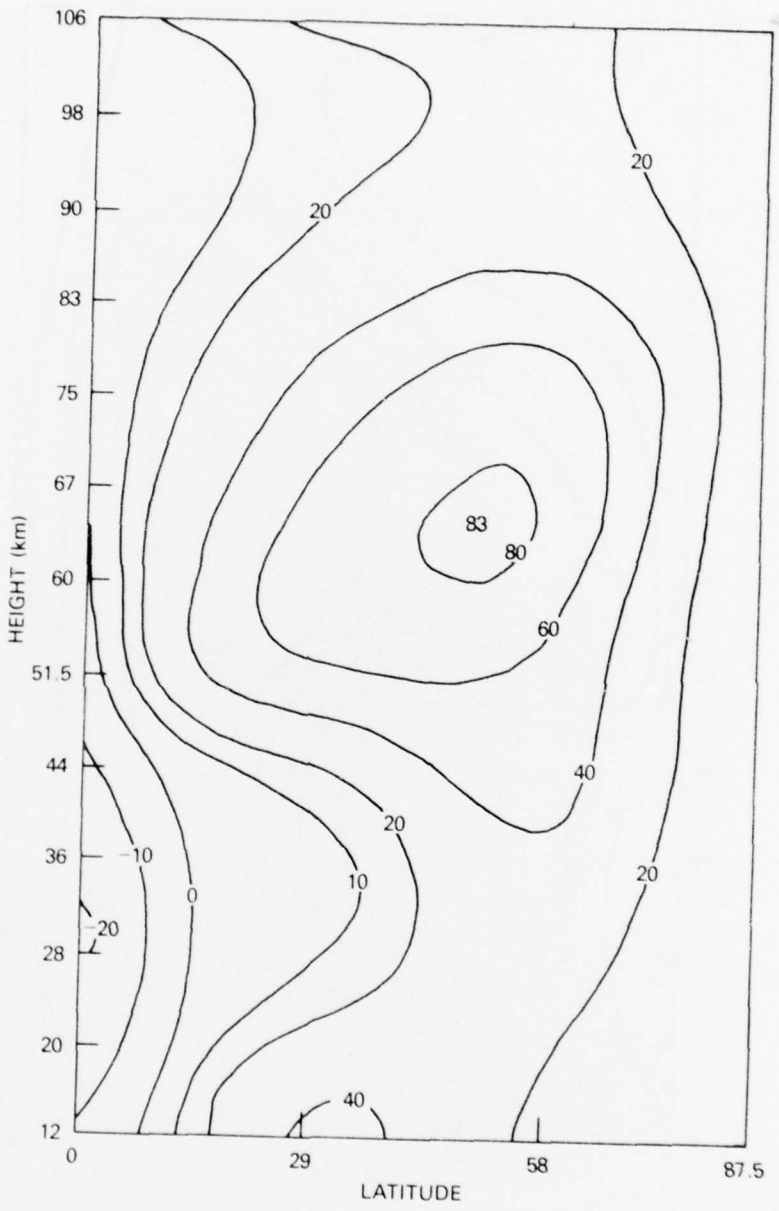

(a)

Fig. 9 — Same as Fig. 3 but $m = 2$, with damping; (a) day 10, (b) day 30, (c) day 40, (d) day 45.

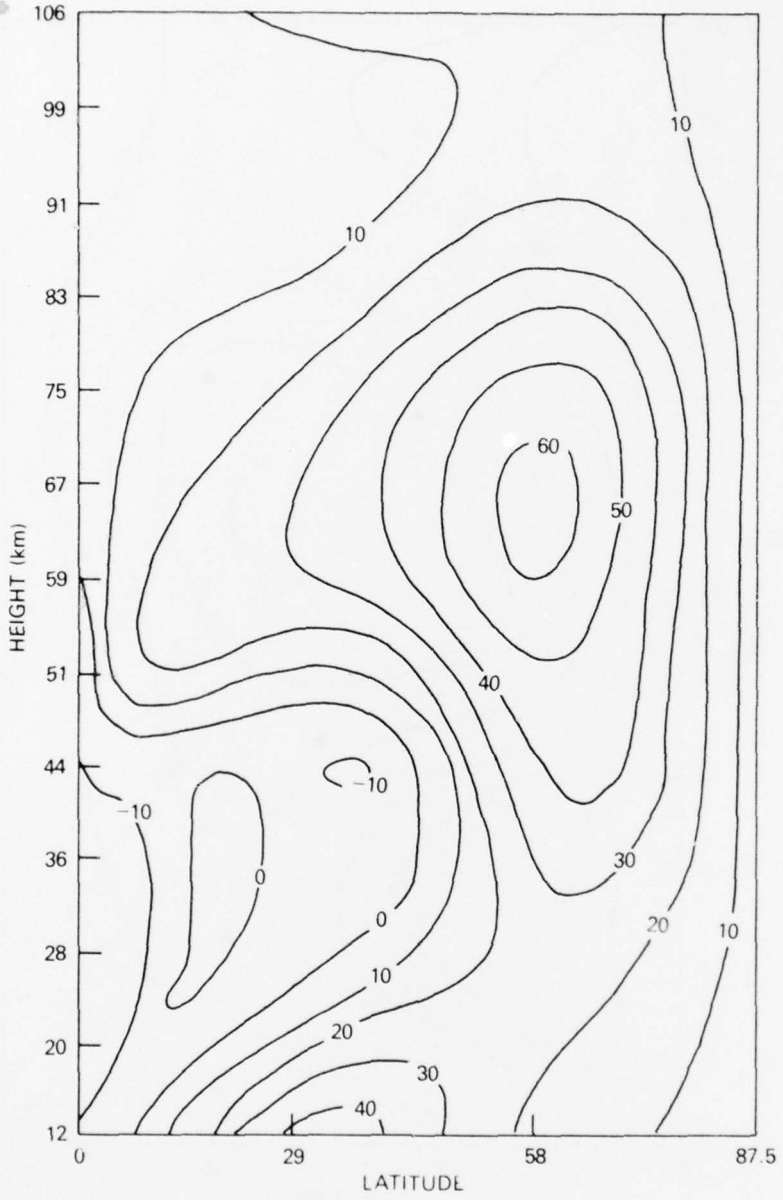

(b)

Fig. 9 (Continued) — Same as Fig. 3 but $m = 2$, with damping; (a) day 10, (b) day 30, (c) day 40, (d) day 45.

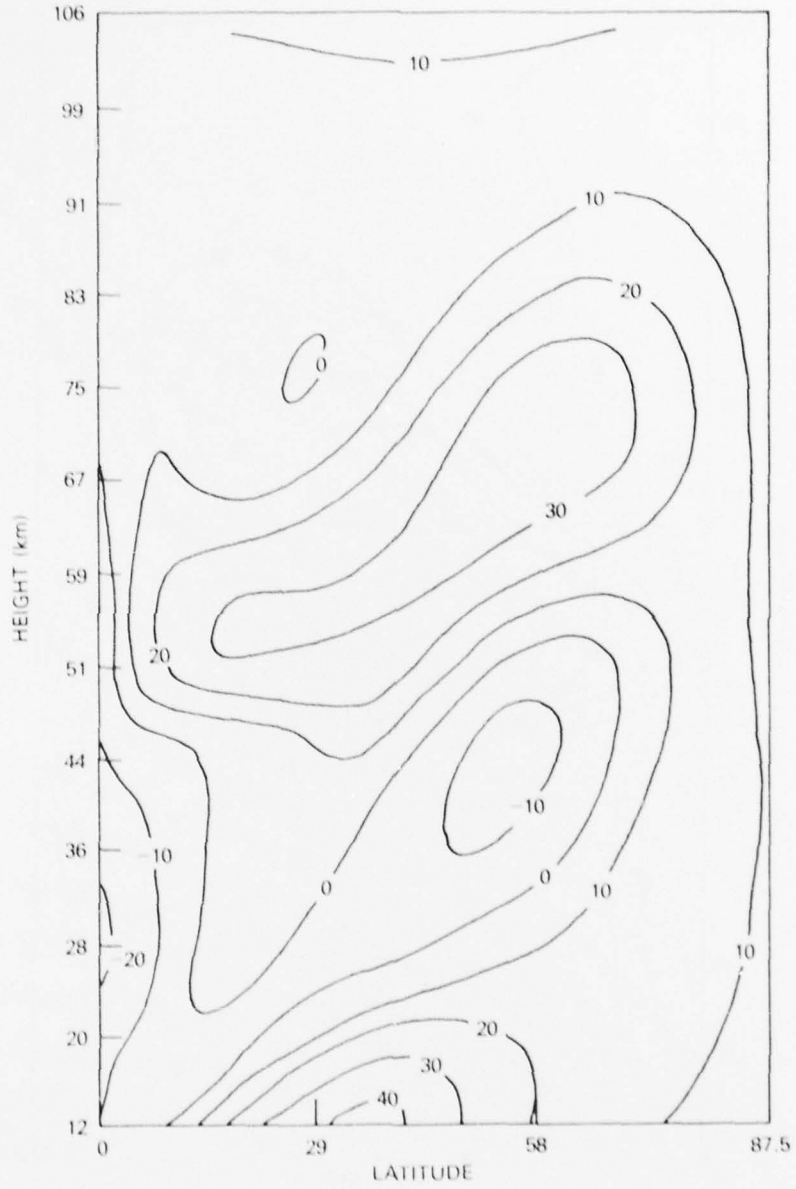

(c)

Fig. 9 (Continued) — Same as Fig. 3 but $m = 2$, with damping. (a) day 10, (b) day 30, (c) day 40, (d) day 45.

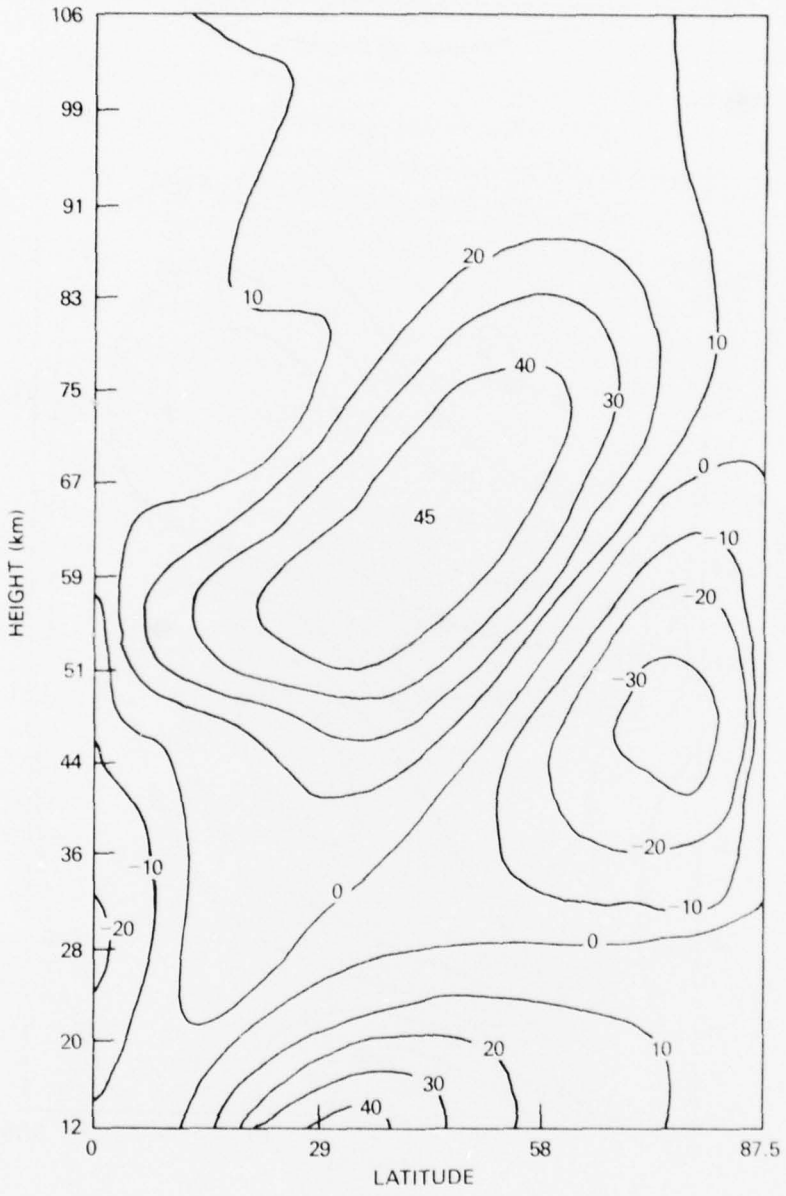

(d)

Fig. 9 (Continued) — Same as Fig. 3 but $m = 2$, with damping; (a) day 10, (b) day 30, (c) day 40, (d) day 45.

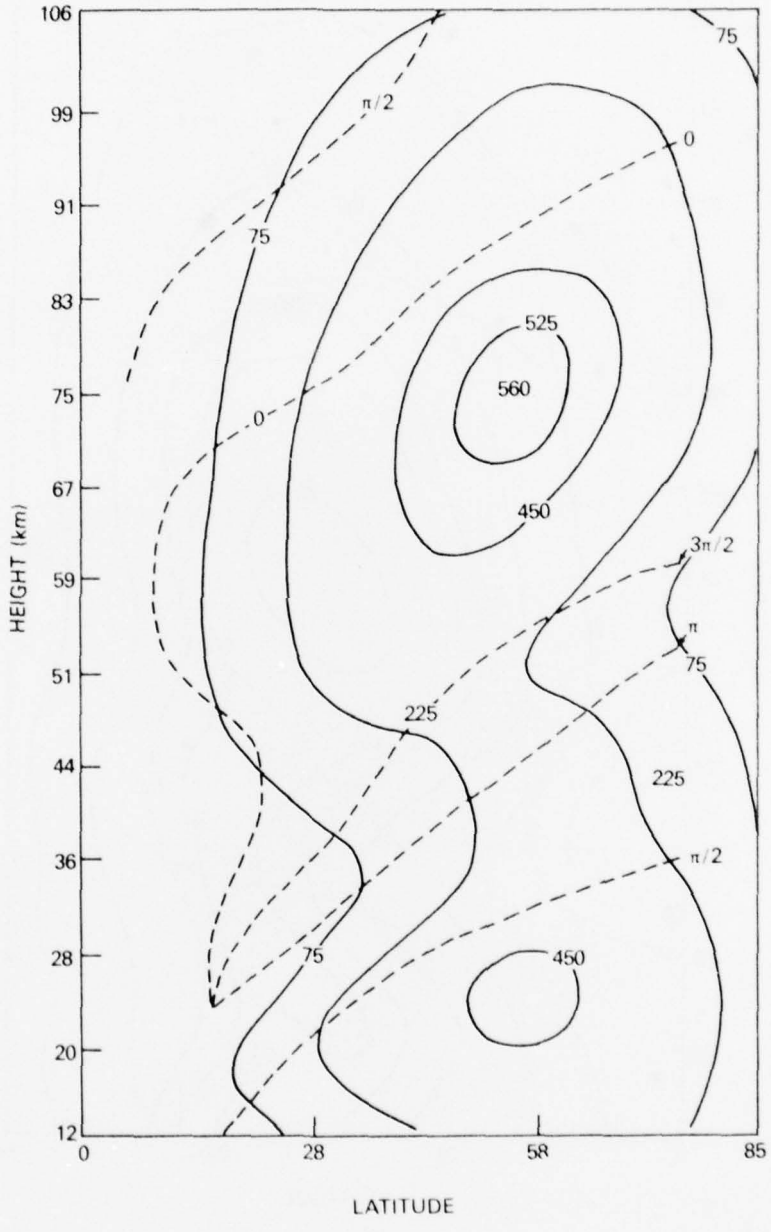

(a)

Fig. 10 — Wave amplitude (gpm) and phase of ϕ' for (a) $m = 1$ and (b) $m = 2$ after 120 and 140 days of integration, respectively.

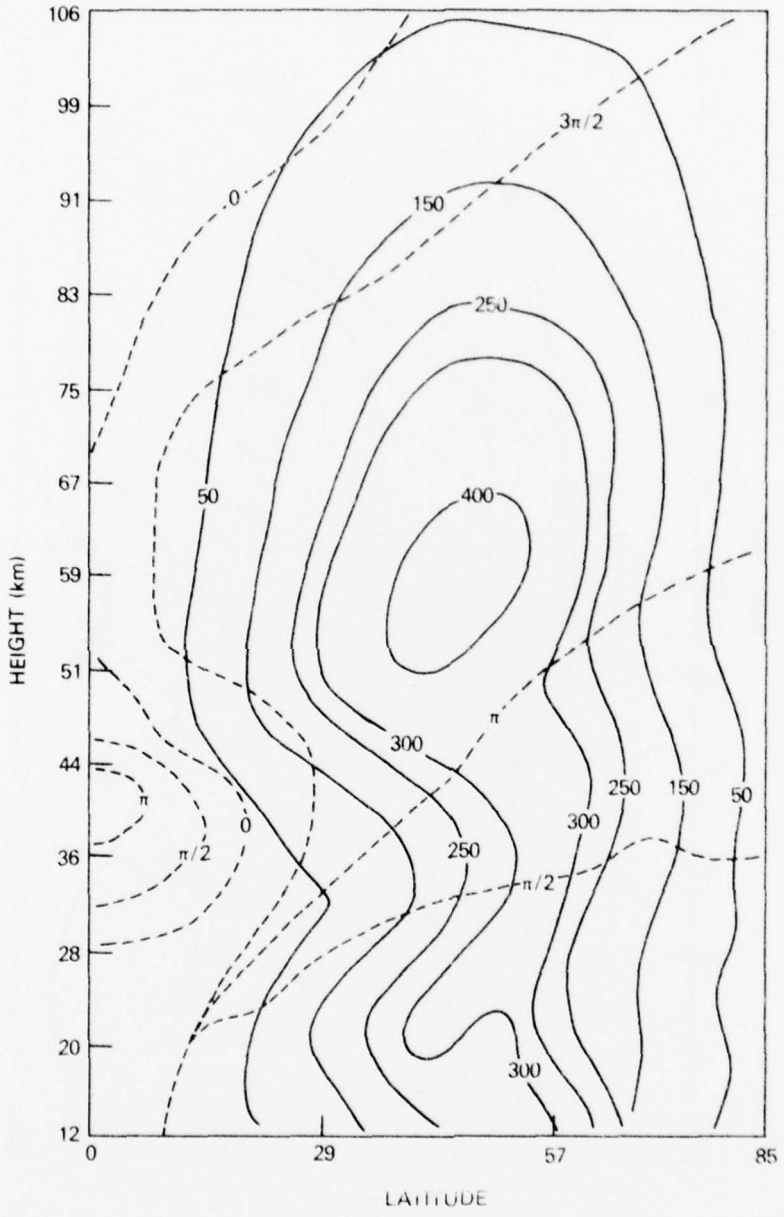

(b)

Fig. 10 (Continued) — Wave amplitude (gpm) and phase of ϕ' for (a) $m = 1$ and (b) $m = 2$ after 120 and 140 days of integration, respectively.

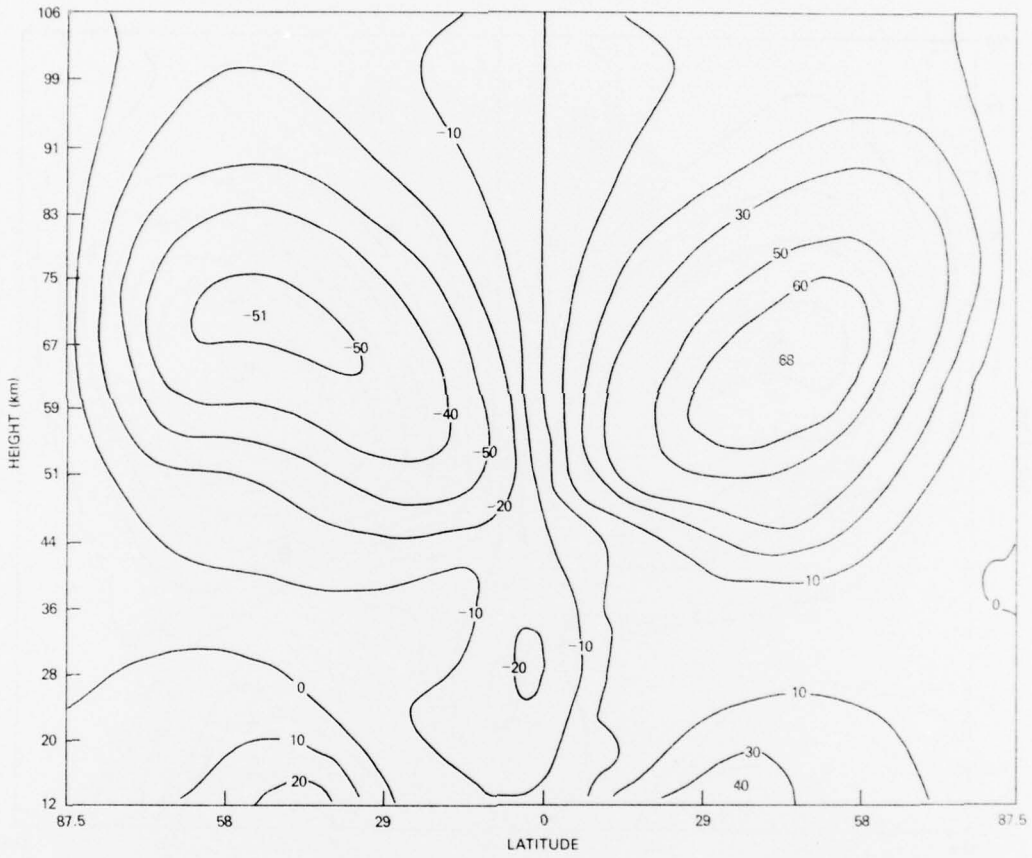

(a)

Fig. 11 — Same as Fig. 10, but mean zonal wind contours after 120 and 140 days of integration from wind field in Fig. 1b.

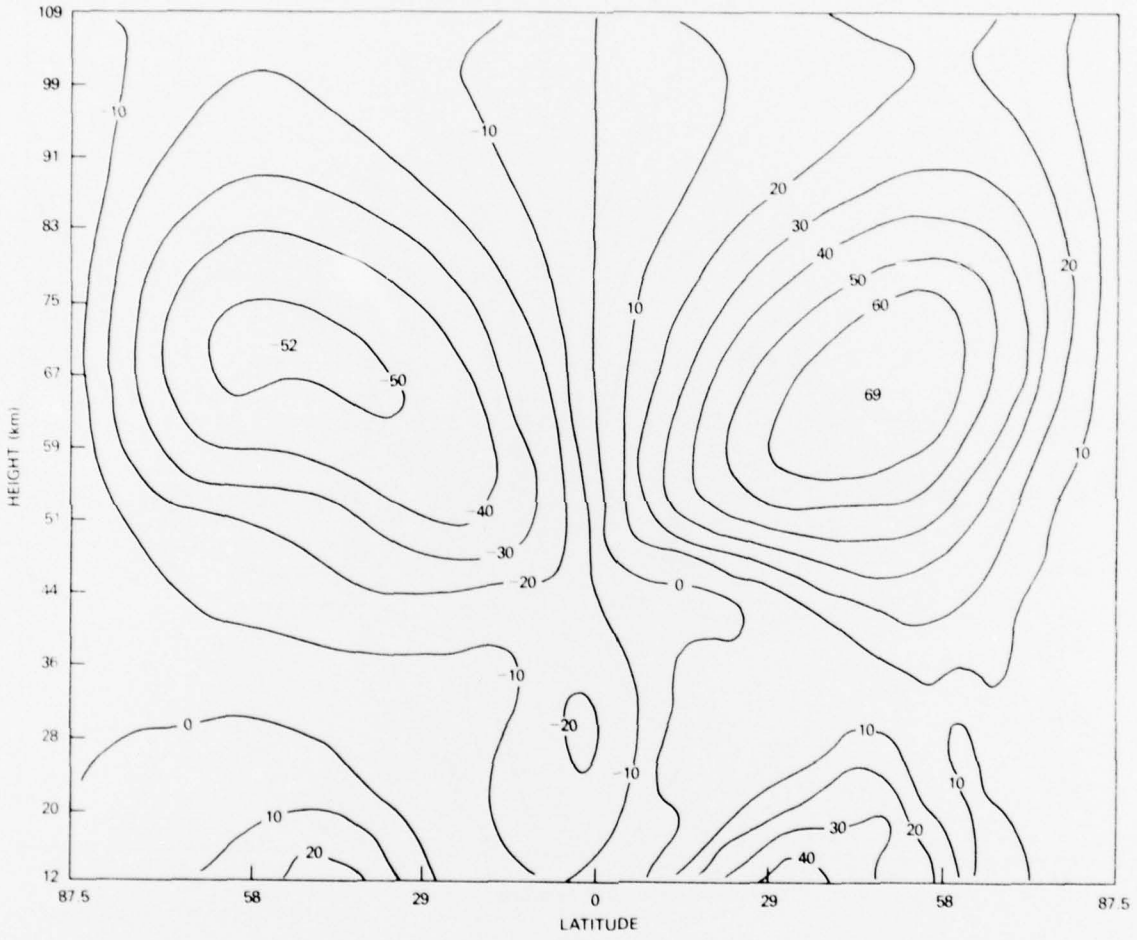

(b)

Fig. 11 (Continued) — Same as Fig. 10, but mean zonal wind contours after 120 and 140 days of integration from wind field in Fig. 1b.

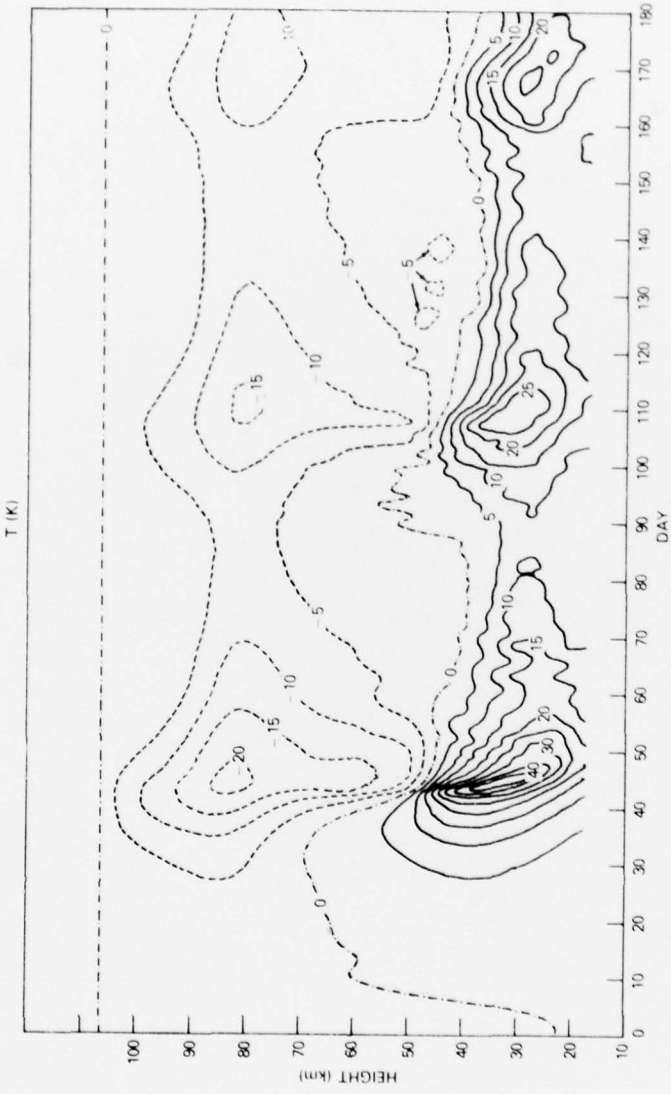

Fig. 12 — Polar temperature changes (ΔT) up to day 180 for $m = 2$